Distinctive dust weather intensities in North China resulted from two types of atmospheric circulation anomalies

Qianyi Huo[1], Zhicong Yin [123], Xiaoqing Ma[1], Huijun Wang[123]

[1]Key Laboratory of Meteorological Disaster, Ministry of Education ~~/ Joint International Research Laboratory of Climate and Environment Change (ILCEC) ~~/ Collaborative Innovation Center on Forecast and Evaluation of Meteorological Disasters ~~(CIC-FEMD)~~, Nanjing University of Information Science & Technology, Nanjing 210044, China
[2] Southern Marine Science and Engineering Guangdong Laboratory (Zhuhai), Zhuhai, China
[3]Nansen-Zhu International Research Centre, Institute of Atmospheric Physics, Chinese Academy of Sciences, Beijing, China

Correspondence to: Zhicong Yin (yinzhc@nuist.edu.cn)

Abstract. Dust weather in North China (NC) has worsened in recent years, posing adverse impacts on the environment, human health, and the economy. A super dust storm occurred on 15 March 2021 raised Beijing's PM_{10} (particulate matter with a diameter less than 10 μm) concentrations above 7000 μg m^{-3}, while 2023 witnessed the highest spring dust weather frequency in nearly a decade. Previous research has primarily focused on the role of the Mongolian cyclone in influencing dust weather in NC, with less attention given to other synoptic systems. Additionally, the differences in PM_{10} concentrations in NC caused by different synoptic systems have not yet been quantified. This study demonstrates that the Mongolian cyclone was responsible for 61.7% of the dust weather in NC, while the remaining 38.3% was primarily caused by the cold high. The dust intensity induced by the Mongolian cyclone was stronger than that of the cold high, with average maximum PM_{10} concentrations of 3076 μg m^{-3} and 2391 μg m^{-3}, respectively. The three-dimensional structure of atmospheric circulation anomalies and related dynamic mechanisms of the two types were concluded. To comprehensively forecast the two types of dust weather, a common predictor was constructed based on the 500 hPa cyclonic anomaly and anticyclonic anomaly circulation systems. These findings contribute to enhancing the comprehension of dust weather in NC and offer insights for both dust weather forecasting and climate prediction.

~~Dust weather in North China (NC) has worsened in recent years, posing adverse impacts on the environment, human health, and the economy. In 2021, the "3.15" super dust storm raised Beijing's PM_{10} (particulate matter with a diameter less than 10 μm) concentrations above 7000 μg m^{-3}, while 2023 witnessed the highest spring dust weather frequency in nearly a decade. Although previous studies have proposed that synoptic systems such as the Mongolian cyclone and cold high can induce dust weather in NC, there has been less focus on the cold high. Furthermore, the differences in PM_{10} concentrations in NC caused by the two synoptic systems have not been quantified. This study demonstrates that the Mongolian cyclone was responsible for 62.4% of the dust weather in NC, while the remaining 37.6% was primarily caused by the cold high. The dust intensity induced by the Mongolian cyclone was stronger than that of the cold high, with average maximum PM_{10} concentrations of 3076 μg m^{-3} and 2391 μg m^{-3}, respectively. The three-dimensional structure of atmospheric circulation anomalies and related dynamic mechanisms of the two types were concluded. A common predictor of the two dust weather types has also been~~

~~identified. These findings contribute to enhancing the comprehension of dust weather in North China and offer valuable insights for both dust weather forecasting and climate prediction.~~

1 Introduction

Dust weather frequently occurs in spring over the northern region of China ~~r North China (NC)~~ and has a number of negative effects on the environment, human health and economy. The strong wind which induces the dust weather, has the potential to inflict severe damage on infrastructure and results in soil erosion, thereby exerting detrimental effects on agricultural productivity (Ahmadzai et al., 2023). Simultaneously, the entrainment of dust particles by the strong wind leads to an increase of PM_{10} (particulate matter with a diameter less than 10 μm) concentration (Krasnov et al., 2016), which reduces air quality and poses a threat to human health, increasing the risk of respiratory and cardiovascular diseases (Lwin et al., 2023). Besides, dust aerosols reduce visibility (Gui et al., 2022), impeding people's travel and adversely affecting traffic safety. ~~In response to global warming, extreme weather has been intensifying and occurring more frequently in China (Yin et al., 2023b).~~

North China (NC; 34–42°N, 105–120°E) is the region, apart from Northwest China, where spring dust weather is most frequent, intense, and has the highest average PM_{10} concentration (Li et al., 2022; Zhang et al., 2023). In contrast to previous studies that examined dust weather across the entire northern region of China, this study specifically focuses on NC. With a dense population, developed economy, and playing a vital role in China's economy, politics, culture, and agriculture, studying dust weather in NC is of great importance. In response to global warming, extreme weather has been intensifying and occurring more frequently in China (Yin et al., 2023b). Severe dust storm reoccurred in the spring of 2021 after an absence for more than 10 years in NC (Zhang et al., 2022). During 14–16 March 2021, the hourly observed PM_{10} concentration exceeded the monitoring threshold in ~~Ordos~~ Ulanqab (>9985 μg m^{-3}) and reached extraordinarily high value in Beijing (>~~76~~400 μg m^{-3}; ~~Filonchyk~~Yin et al., 202~~2+~~). In the spring of 2023, there was a notable increase in the frequency of dust weather, reaching the highest level observed in recent decades (Yin et al., 2023a). ~~The severe dust storm event during 19–24 March 2023 impacted a large range of area, covering over 4.8 million km^2 (Yin et al., 2023a). In general, the dust weather in NC during 2021 and 2023 exhibited characteristics of high intensity, frequent occurrence, and extensive impact.~~

The generation of dust weather requires both dust source conditions and dynamic conditions. The primary dust sources of dust weather include deserts and sandy areas in arid and semi-arid regions (Huang et al., 2014). In East Asia, the Gobi Desert located in the Mongolian Plateau and northern China is a major source of sandstorms (Zhang et al., 2023). In recent years, China has made significant progress in combating land desertification (Zhang and Huisingh, 2018). However, during the dust weather events in March and April 2023, over 42% of the dust concentration in NC originated from cross-border transport from Mongolia (Chen et al., 2023a). Strong winds and thermally unstable atmospheric stratification were the primary dynamic conditions for the formation of dust weather (Wu et al., 2023), which facilitated the entrainment and uplift of dust particles (Zhao et al., 2022). The intensity of turbulence and the structure of the boundary layer affect the lifting and diffusion capabilities of sand and dust (Shao, 2008). The combined effect of thermal (i.e., unstable stratification) and dynamic (i.e., near-

surface wind shear) factors enhances turbulent motion, leading to increased wind erosion, which favors the lifting of sand and dust (Wiggs, 2011).

The long-distance transport of dust aerosols in the lower atmosphere is regulated by regional synoptic systems (Huang et al., 2014). Meanwhile, the frequent dust weather activities in East Asia ~~during~~ in spring are closely related to mid-latitude synoptic-scale cyclone activities (Qian et al., 2002). The Mongolian cyclone is the primary synoptic system causing dust weather in NC (Li et al., 2022). Both the severe dust storm events on 15 March 2021 and on 22 March ~~-~~2023 were attributed to the Mongolian cyclone (Mu et al., 2023; Yin et al., 2023a). The appearance of the Mongolian cyclone triggered strong gusts and unstable thermal conditions, disturbed loose surfaces, and lifted surface dust into the air through upward motion (Tian et al., 2023). As the Mongolian cyclone moved eastward, the northerly winds behind it transported dust from the source area southward, thereby affecting NC (Takemi and Seino, 2005).

Recent weather and climate studies on the atmospheric circulation systems related to dust weather in NC have primarily focused on the frequency, intensity, and physical processes of the Mongolian cyclone (Wu et al., 2016; Bueh et al., 2022; Chen et al., 2023b; Gao et al., 2024). However, the Mongolian cyclone alone cannot explain all instances of dust weather. ~~A dust weather event in NC on 14 March 2023, caused by a cold high (Fig. S1a), resulted in relatively low PM_{10} concentrations at 1247 μg m^{-3} (Fig. S2). This dust weather event went largely unnoticed. Subsequently, on 22 March, a severe dust storm was brought by the Mongolian cyclone (Fig. S1b). This dust weather led to higher PM_{10} concentrations at 9993 μg m^{-3} (Fig. S2), which garnered more attention~~ According to the daily maximum observed PM_{10} concentration in NC, a dust event caused by a cold high resulted in a relatively low PM_{10} concentration of 1247 μg m^{-3} on 14 March 2023 (Fig. S1a). This event went largely unnoticed. However, on 22 March 2023, a severe dust storm, brought by a Mongolian cyclone (Fig. S1b), led to higher PM_{10} concentrations of 9993 μg m^{-3}, garnering more attention (Yin et al., 2023a). Research on subjective and objective classifications of dust weather has been conducted (Liu et al., 2004; Yun et al., 2013; Yi et al., 2021). ~~(Yin et al., 2023a). Liu et al. (2004) and Yun et al. (2013) subjectively classified dust storms in NC based on atmospheric circulation, while Yi et al. (2021) used the K-means clustering method to classify circulation patterns of dust weather in the entire northern region of China.~~ These studies indicate that besides the Mongolian cyclone, other synoptic systems such as the cold high also played significant roles in causing dust weather in North China.~~They all found that besides the Mongolian cyclone, the cold high and associated cold front also played significant roles in causing dust weather in NC.~~

This study used PM_{10} concentrations as indicators to investigate the differences in the intensity of dust weather caused by the Mongolian cyclone and other synoptic systems. The differences and similarities in atmospheric circulation anomalies between the two types were compared. In order to comprehensively predict both types of dust weather, common anomalous circulation systems for the two types have been identified, and a common predictor has been established. This study helps enhance the understanding of dust weather in NC and provides references for dust weather forecasting and climate prediction.~~What are the differences in PM_{10} concentration and frequency of dust weather caused by the Mongolian cyclone and cold high? What atmospheric circulation and dynamic mechanisms are responsible for the two types of dust weather? Is~~

there any predictor that can forecast dust weather in NC? This study aims to address the above questions, not only to enhance understanding of the NC dust weather but also to provide references for dust weather forecasting and climate prediction.

2 Data and method

2.1 Data

Hourly observed station PM_{10} and $PM_{2.5}$ concentrations in March, April and May from 2015 to 2023 are derived from China National Environmental Monitoring Centre and publicly accessible at https://quotsoft.net/air/. The study area is located in NC, specifically within the range of 34–42°N, 105–120°E. PM_{10} and $PM_{2.5}$ concentration data from 556 stations in NC have been utilized for selecting dust weather days, with negative and missing values excluded. The fifth generation European Center for Medium Range Weather Forecasts (ERA5) provided hourly reanalysis meteorology data with the horizontal resolution of 0.25°×0.25° on pressure and surface levels in spring (March, April and May) from 2015 to 2023 (Hersbach et al., 2023). Data at 8:00, 12:00, 16:00, 20:00 (Beijing local time) are selected to calculate the daily mean values. The variables include geopotential height at 500 hPa (Z500), zonal and meridional winds at 10 m (UV10), zonal and meridional winds at 850 hPa (UV850), zonal winds at 200 hPa (U200), sea level pressure (SLP), temperature at 1000 hPa (T1000), temperature at 850 hPa (T850), vertical velocity at 500 hPa (ω500), 10 m wind gust (Gust10), surface air temperature (SAT), planetary boundary layer height (PBLH), and vertical velocity (ω), zonal and meridional winds, divergence (div), specific humidity (q) from 1000 hPa to 200 hPa on 23 pressure levels.

Hourly observed station PM_{10} concentrations in March, April and May from 2015 to 2023 are derived from China National Environmental Monitoring Centre and publicly accessible at https://quotsoft.net/air/. The Normalized Difference Vegetation Index (NDVI) quantifies the vegetation by measuring the difference between near-infrared and red light. Gridded NDVI data, with a horizontal resolution of 1°×1° in March 2023 were obtained from the National Oceanic and Atmospheric Administration's (NOAA) National Centers for Environmental Information (Vermote, 2019). The Copernicus Climate Change Service (C3S, 2018) produced provided seasonal forecast products from European Centre for Medium-Range Weather Forecasts (ECMWF) SEAS5.1, Deutscher Wetterdienst (DWD) GCFS2.0 & GCFS2.1, and Météo-France (MF) System6 & System7 & System8. comprising a total of 25 ensemble members. In this study, the Z500 and SLP data for spring were initialized annually on February 1st (one-month lead) with a temporal resolution of 12 hours and a spatial resolution of 1°×1°. The daily ensemble mean data for each variable is used in this study.

2.2 Method

The maximum PM_{10} concentration serves as an indicator of dust weather intensity, reflecting the greatest impact of dust weather on NC (34–42°N, 105–120°E). The changes in daily maximum PM_{10} concentrations observed in NC during spring 2015–2023 are illustrated in Figure S2. The first and third quartiles of the PM_{10} concentration series during spring 2015–2023

~~were 426.5 μg m^{-3} and 1019 μg m^{-3}, respectively. Referring to selected percentile values, two PM_{10} concentration thresholds were chosen at 500 μg m^{-3} and 1000 μg m^{-3}. Periods when PM_{10} concentrations exceeded 1000 μg m^{-3} were defined as high concentration periods, while periods below 500 μg m^{-3} were categorized as low concentration periods. It can be observed that the spring PM_{10} concentrations exhibited distinct periods of high and low concentrations. The high concentration periods had relatively short durations (i.e., average of 1.97 days), while the low concentration periods had relatively longer durations (i.e., average of 2.39 days). During high PM_{10} concentration periods, there were sharp increases in PM_{10} concentrations. In this study, the dates corresponding to the maximum PM_{10} concentrations during high PM_{10} concentration periods were defined as Dust days (Fig. S2). Conversely, the dates corresponding to the minimum PM_{10} concentrations during low PM_{10} concentration periods were defined as Non-Dust days (Fig. S2).~~

During dust events, PM_{10} concentrations significantly increase, at least doubling or even increasing by tens of times (Dulam et al., 2014). In this study, the maximum PM_{10} concentration was utilized to confirm the occurrence of dust weather in NC. In order to better identify dust days, the daily maximum PM_{10} concentrations were selected from the actual hourly observed values for each station in NC. The station with the highest PM_{10} concentration in NC was chosen, and the maximum value at that station was used as a reference for selecting dust day. The changes in daily maximum PM_{10} concentrations observed in NC during spring 2015–2023 are illustrated in Fig. S2. The first and third quartiles of the PM_{10} concentration series in spring 2015–2023 were 426.5 μg m^{-3} and 1019 μg m^{-3}, respectively. Referring to selected percentile values, two PM_{10} concentration thresholds were chosen at 500 μg m^{-3} and 1000 μg m^{-3}. Periods when PM_{10} concentrations exceeded 1000 μg m^{-3} were defined as high concentration periods, while periods below 500 μg m^{-3} were categorized as low concentration periods. In this study, the dates corresponding to the maximum PM_{10} concentrations during high PM_{10} concentration periods were designated as Dust days (Fig. S2), representing days most significantly impacted by dust in NC during dust events. Conversely, the dates corresponding to the minimum PM_{10} concentrations during low PM_{10} concentration periods were designated as Non-Dust days (Fig. S2).

Considering potential anthropogenic influences, the $PM_{2.5}$ concentrations were obtained at the same site and time as the maximum PM_{10} concentrations on the Dust days, and the $PM_{2.5}/PM_{10}$ ratios were calculated. A lower $PM_{2.5}/PM_{10}$ ratio indicates the presence of a significant amounts of coarse particles in the air, associated with natural sources such as dust storms, while a higher $PM_{2.5}/PM_{10}$ ratio suggests pollution from anthropogenic sources (Sugimoto et al., 2016). In NC, the average $PM_{2.5}/PM_{10}$ ratio typically ranges from 0.5 to 0.7 and exhibits distinct seasonal variations, being lower in spring (Wang et al., 2015). To eliminate the influence of anthropogenic aerosols, two days were excluded from the selected Dust days as their $PM_{2.5}/PM_{10}$ ratio exceeded 0.5.

According to the synoptic definition of the extratropical cyclone (Shou, 2006), the Mongolian cyclone was identified based on the following criteria: (1) The lowest SLP within the range of 40–55°N, 100–130°E should not exceed 1010 hPa. (2) The average pressure gradient within a ±2.5° latitude and longitude range around the lowest SLP must be equal to or greater than 0.55 hPa per 100 km. ~~a Mongolian cyclone is identified by a central sea level pressure within the region of 40–55°N, 100–125°E that does not exceed 1010 hPa and is lower than the sea level pressure at the surrounding eight grid points.~~

~~Furthermore, the average pressure gradient in a 5×5 grid centered around the cyclone should be equal to or greater than 0.55 hPa per 100 km.~~ The vertical air temperature difference (VATD) was defined as T1000–T850, which indicate~~s~~d the thermal atmospheric instability. The vertical transport of westerly momentum was defined as $\partial(u\omega)/\partial P$, $\partial(u\omega)/\partial P < 0$ represents downward fluxes (Zhong et al., 2019). The composites of the variables were computed based on the daily mean values. All anomalies were calculated relative to the daily mean values in spring from 2015 to 2023. The correlation coefficients in this study were calculated using Pearson correlation.

3 PM_{10} concentration~~s~~ differences ~~related to~~between ~~-~~regional synoptic systems

~~The maximum PM_{10} concentration serves as an indicator of dust weather intensity, reflecting the greatest impact of dust weather on NC (34–42°N, 105–120°E). The changes in daily maximum PM_{10} concentrations observed in NC during spring 2015–2023 are illustrated in Figure S2. The first and third quartiles of the PM_{10} concentration series during spring 2015–2023 were 426.5 μg m^{-3} and 1019 μg m^{-3}, respectively. Referring to selected percentile values, two PM_{10} concentration thresholds were chosen at 500 μg m^{-3} and 1000 μg m^{-3}. Periods when PM_{10} concentrations exceeded 1000 μg m^{-3} were defined as high concentration periods, while periods below 500 μg m^{-3} were categorized as low concentration periods. It can be observed that the spring PM_{10} concentrations exhibited distinct periods of high and low concentrations. The high concentration periods had relatively short durations (i.e., average of 1.97 days), while the low concentration periods had relatively longer durations (i.e., average of 2.39 days). During high PM_{10} concentration periods, there were sharp increases in PM_{10} concentrations. In this study, the dates corresponding to the maximum PM_{10} concentrations during high PM_{10} concentration periods were defined as Dust days (Fig. S2). Conversely, the dates corresponding to the minimum PM_{10} concentrations during low PM_{10} concentration periods were defined as Non-Dust days (Fig. S2).~~

The primary surface synoptic system leading to dust weather in NC was the Mongolian cyclone ~~(Li et al., 2022)~~. Additionally, other synoptic ~~cold high~~ systems ~~along with accompanying cold fronts~~ could also contribute to dust weather affecting NC (Liu ~~Yun~~ et al., ~~2013~~2004). By objectively identifying the presence of the Mongolian cyclone, Dust days ~~can be~~were further classified into two categories. As depicted in the ~~composite~~ original SLP fields for the two types, the main surface synoptic systems for the two types of Dust days were the Mongolian cyclone and cold high respectively~~the main surface synoptic systems for the two types of Dust days were the Mongolian cyclone and cold high~~ (Fig. ~~S1c~~S1c, ~~d~~d). Therefore, the two types of Dust days were respectively named Mongolian Cyclone (MC) type and Cold High (CH) type. Dust days caused by Mongolian cyclones (MC type) accounted for a significant portion during the spring seasons from 2015 to 2023, at 61.7%. Other synoptic systems, mainly cold high systems (CH type), accounted for 38.3% of the total Dust days. ~~From 2015 to 2023, Dust days in April and May were more frequent compared to March (Fig. 1a). The highest number of Dust days occurred in May, followed by April, with March having the fewest occurrences (Fig. 1a). The MC type was the predominant weather pattern causing dust weather in NC during 2015–2023, accounting for 62.4% of the total days in spring (Fig. 1a). In May, the proportion of MC days was the highest at 71.7%, followed by April at 57.9%, and March at the lowest with 53.8%~~

~~(Fig. 1a).~~ Figure 1c illustrates the temporal distribution of MC days, CH days, and Non-Dust days in spring from 2015 to 2023. ~~It was evident that the two types of Dust days exhibited discontinuous characteristics in time each year.~~

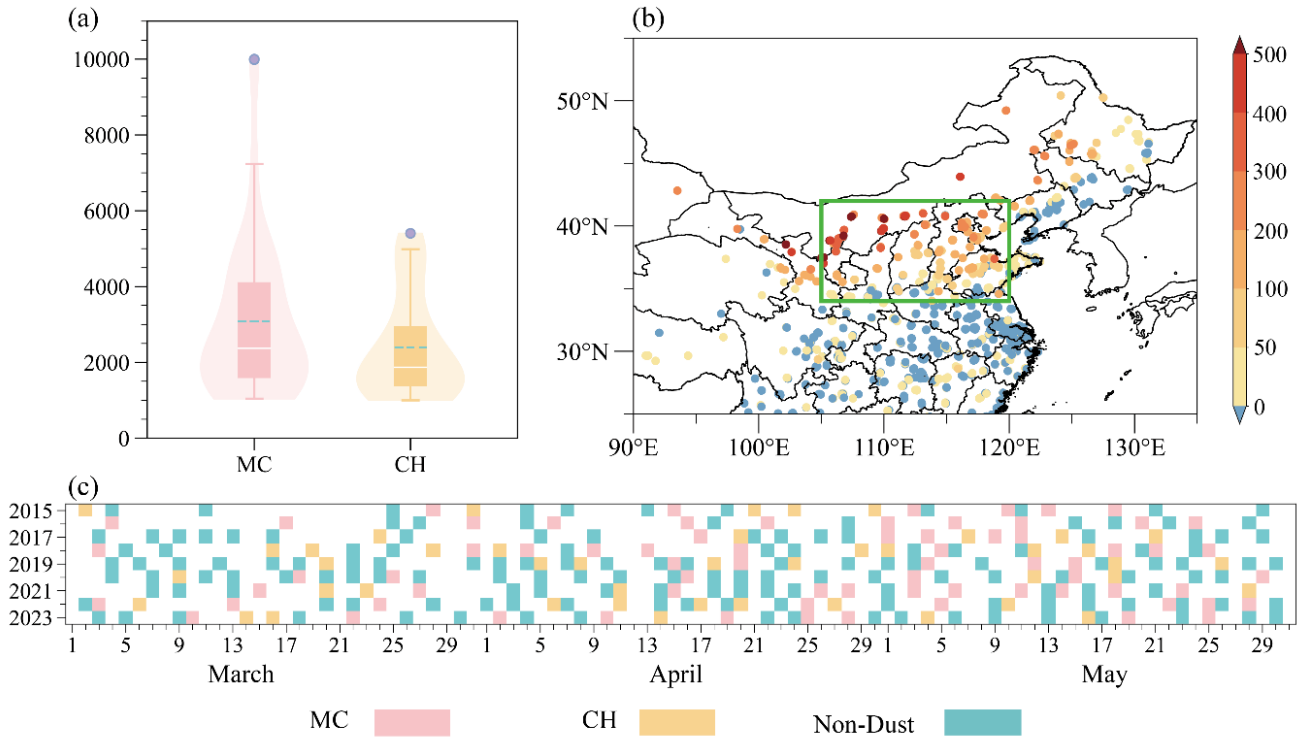

Figure 1. (a) Boxplots of daily maximum PM_{10} concentrations (units: μg m^{-3}) in NC during MC days (pink) and CH days (orange). The cyan dashed lines and blue dots in the boxplot represent average PM_{10} concentrations and outlier values. Density distributions of PM_{10} concentrations are shown by pink and orange shadings for MC days and CH days respectively. (b) The composite differences of observed daily maximum PM_{10} concentrations (scatter, units: μg m^{-3}) during MC days relative to CH days. The green box indicates NC. (c) The temporal distribution of MC days, CH days and Non-Dust days in spring from 2015 to 2023.

There are distinct differences in PM_{10} concentrations between the MC and CH types. Both of the two types ~~the MC type and CH type~~ exhibited high PM_{10} concentrations in NC (Fig. S3~~3c, d~~). Compared to the CH type, the MC type resulted in higher PM_{10} concentrations and showed more pronounced extremes (Fig. 1a~~b~~). The outliers in the PM_{10} concentration boxplot for MC type in Fig. ~~1b~~ 1a included the severe dust storms on March 15 2021, and March 22 2023~~, reflecting the extremity of these two dust events~~. During Dust days, the dust particles that caused the increase in PM_{10} concentrations originated from the dust source area. From the NDVI, it can be observed that there was a significant lack of vegetation cover in the northwest direction outside NC (Fig. ~~S3a~~S3a). This area (NDVI < 0.1), serving as an external dust source region, could provide favorable conditions for dust emissions (Wang et al., 2021). From the spatial distribution differences in PM_{10} concentrations, it can be observed that the MC type resulted in relatively higher PM_{10} concentrations in NC, especially in its northern region (Fig. 1b).~~From the spatial distribution differences in PM_{10} concentrations, it can be observed that the MC type resulted in relatively~~

higher PM_{10} concentrations in the northern part of NC, especially near the vicinity of the dust source area (Fig. 1b). Additionally, the Northeast China also experienced significant impacts during MC days (Fig. 1b). In contrast, the CH type led to higher PM_{10} concentrations in the southern part of NC and further southward areas, with the influence of dust particles leaning more towards the south compared to MC days (Fig. 1b).

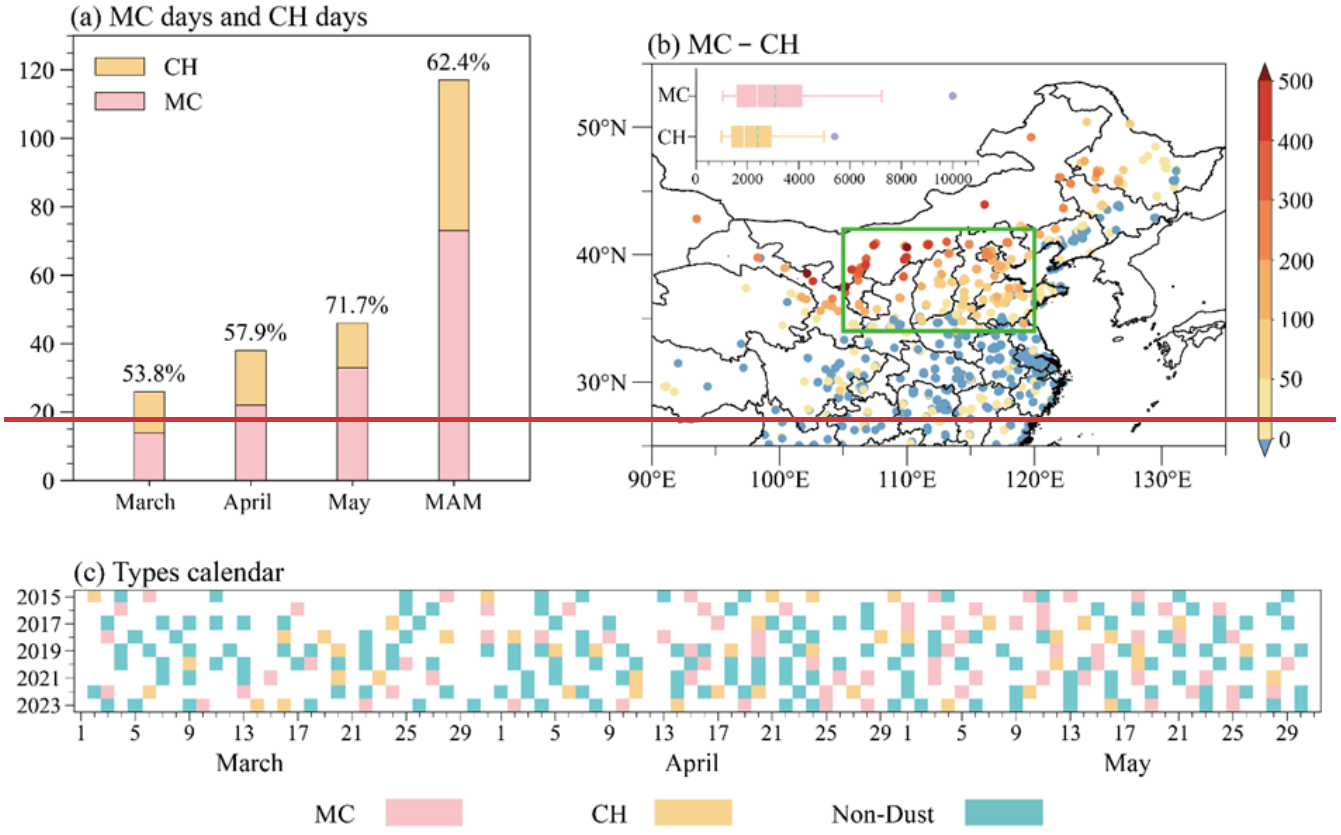

Figure 1. (a) The cyan dashed lines and blue dots in the boxplot represent average PM_{10} concentrations and outlier values. The number of Dust days (stacked bar) in March, April, May and MAM (March, April and May) from 2015 to 2023. The pink parts and orange parts represent the number of MC days and CH days respectively. The proportions depicted above the bars indicate the percentages of MC days within Dust days. (b) The composite differences of observed daily maximum PM_{10} concentrations (scatter, units: $\mu g\ m^{-3}$) during MC days relative to CH days. The green box indicates NC. The boxplot in the top left corner indicates daily maximum PM_{10} concentrations (units: $\mu g\ m^{-3}$) of MC days (pink) and CH days (orange). The cyan dashed lines and blue dots in the boxplot represent average PM_{10} concentrations and outlier values. (c) The temporal distribution of MC days, CH days and Non-Dust days in spring from 2015 to 2023.

4 Large-scale atmospheric circulation anomalies~~and associated dynamic mechanisms~~

During Dust days of MC and CH types, there were strong anomalous northerly winds to the north of NC at the surface (Fig. 2d, e). During MC days, due to the presence of the Mongolian cyclone (Fig. S1c), there was a significant negative SLP anomaly in the eastern part of East Asia, with a positive anomaly in the west (Fig. 2a). The rear part of the low-pressure anomaly exhibited strong anomalous northwest winds (Fig. 2d). During CH days, the northern part of East Asia exhibited a significant cold high-pressure anomaly, with a low-pressure anomaly in the south (Fig. 2b). Between the two anomalous circulations, there were northeasterly anomalous winds to the north of NC (Fig. 2e). The easterly wind anomaly components weakened the westerly wind components of the surface winds in the CH type. For CH days, the actual wind direction was more northerly compared to MC days (Fig. S1c, d).

Compared to the CH type, the MC type exhibited stronger dynamic instability, manifested by higher anomalies in Gust10 (Fig. S4a, b). Additionally, the increase in VATD favored atmospheric thermal instability in NC and the surrounding external dust source areas (Fig. S4a, b). The combination of dynamic and thermal instability enhanced turbulence in the atmospheric boundary layer (Garratt, 1992). The anomalously intensified turbulence aided in lifting surface dust particles into the atmosphere (Wiggs, 2011), while also elevating the PBLH in NC and the surrounding external dust source areas (Fig. S4c, d). The higher PBLH provided favorable conditions for the dispersion of dust particles from external dust source areas towards NC (Shao, 2008). It is observed that there were anomalous divergent winds over the external dust source areas on MC and CH days (Fig. 2d, e). The anomalous northerly wind facilitated the transport of dust particles from external dust source areas to NC (Fig. 2d, e), leading to the increase in PM_{10} concentrations. The anomalous divergent winds not only aided in outward transport of dust particles but also suppressed the transport of moisture towards the dust source areas. This resulted in anomalously dry conditions near the surface of the external dust source areas (Fig. 2d, e), promoting dust emissions.

Although there were significant differences in the surface circulation anomaly patterns between the MC and CH types, some similar features could be observed in the mid to upper troposphere. The MC type and CH type displayed intensified westerly winds over the mid-latitude East Asia region at 200 hPa (Fig. 3a, b). At 500 hPa, both the MC and CH types exhibited cyclonic anomalies to the north of NC and anticyclonic anomalies to the east of NC (Fig. 3a, b). Compared to the CH type, the MC type showed stronger negative geopotential height anomalies at 500 hPa, with the center located in the northern part outside of NC (Fig. 3a). In contrast, the geopotential height anomalies to the north of NC at 500 hPa were weaker for the CH type (Fig. 3b). Since this 500 hPa cyclonic anomaly is located adjacent to the northern part of NC and over the sparsely vegetated external dust source area to the northwest of NC (Fig. S3a), we hypothesize that this 500 hPa cyclonic anomaly (CA) is a key anomalous circulation system influencing dust activities in NC. The vertical circulation structure of CA was further analyzed. During Dust days, CA exhibited an asymmetric vertical structure (Fig. 3d, e). For the MC type, the western part of the CA showed positive ω anomalies, while the eastern part showed negative ω anomalies (Fig. 3d). For the CH type, the positive ω anomalies were more biased towards the northwest of CA, with negative ω anomalies in the southeastern part of CA (Fig. 3e).

The vertical circulation anomalies associated with CA were primarily related to the emission and transport of dust from the external dust source areas outside of NC. The anomalous subsidence facilitated the downward transport of westerly momentum from the upper troposphere to near the surface (Fig. 4a, b), favoring the enhancement of anomalies in V850 and Gust10 (Fig. S4). With the strengthening of westerly momentum exchange, the conversion of kinetic energy toward turbulent flow was enhanced (Liu and Liu, 2011). Furthermore, the anomalous subsidence also helped to transport dry and cold air from the mid-troposphere to layers closer to the surface (Fig. 4d, e). The intrusion of cold air helped to disrupt the stable boundary layer, resulting in increased atmospheric thermal instability and turbulent kinetic energy (Liu and Liu, 2011). The stronger turbulence not only lifted surface dust particles but also led to higher PBLH (Fig. S4c, d). The anomalous divergence in the lower troposphere provided favorable conditions for the outward spread of dust particles (Fig. 4d, e). Anomalous convergence zones promoted the aggregation of dust particles and transported them to higher altitudes through anomalous upward motion (Fig. 4d, e). This prolonged the settling time of dust particles and facilitated their long-distance transport.

The east-west contrast in the vertical structure of the CA was weaker for the CH type compared to the MC type (Fig. S5a), whereas the north-south contrast for the CH type was more pronounced (Fig. 4b, e). For the CH type, the enhanced anomalous meridional vertical circulation increased the importance of the dust source areas to the north of NC (Fig. S3a). The vegetation cover outside of NC along the northern direction was relatively better than that along the northwest direction outside of NC, indicated by higher NDVI (Fig. S3a). This might lead to lower PM_{10} concentrations in NC during CH days compared to MC days. Furthermore, in NC and external dust source areas, meteorological variable anomalies of the CH type exhibited spatial distribution characteristics similar to the MC type, but with weaker intensities (Fig. 2d, e; Fig. S4). Spatial correlation coefficient results indicated a significant correlation between these meteorological variables and the maximum PM_{10} concentrations in NC (Fig. S6). These results partially explained why the PM_{10} concentrations on CH days are lower relative to MC days.

For comparison, the atmospheric circulation anomalies during Non-Dust days were also analyzed. The atmospheric circulation anomalies during Non-Dust days exhibited distribution characteristics opposite to those on Dust days. The southeastern part of East Asia showed positive SLP anomalies, while the northwestern part exhibited negative SLP anomalies and warm anomalies (Fig. 2c). The wind speed anomalies in NC and its surrounding areas were relatively low, with anomalous southerly winds being conducive to the transport of moisture from the south, leading to higher q (Fig. 2f). At 500 hPa, an anticyclonic anomaly was observed to the north of NC, while to the east of NC showed a cyclonic anomaly (Fig. 3c). In the upper troposphere, the westerly winds in the mid-latitudes of East Asia were significantly weakened (Fig. 3c), and the subsidence and downward momentum transport weakened (Fig. 3f, Fig. 4c). These circulation anomalies were unfavorable for the occurrence of dust weather.

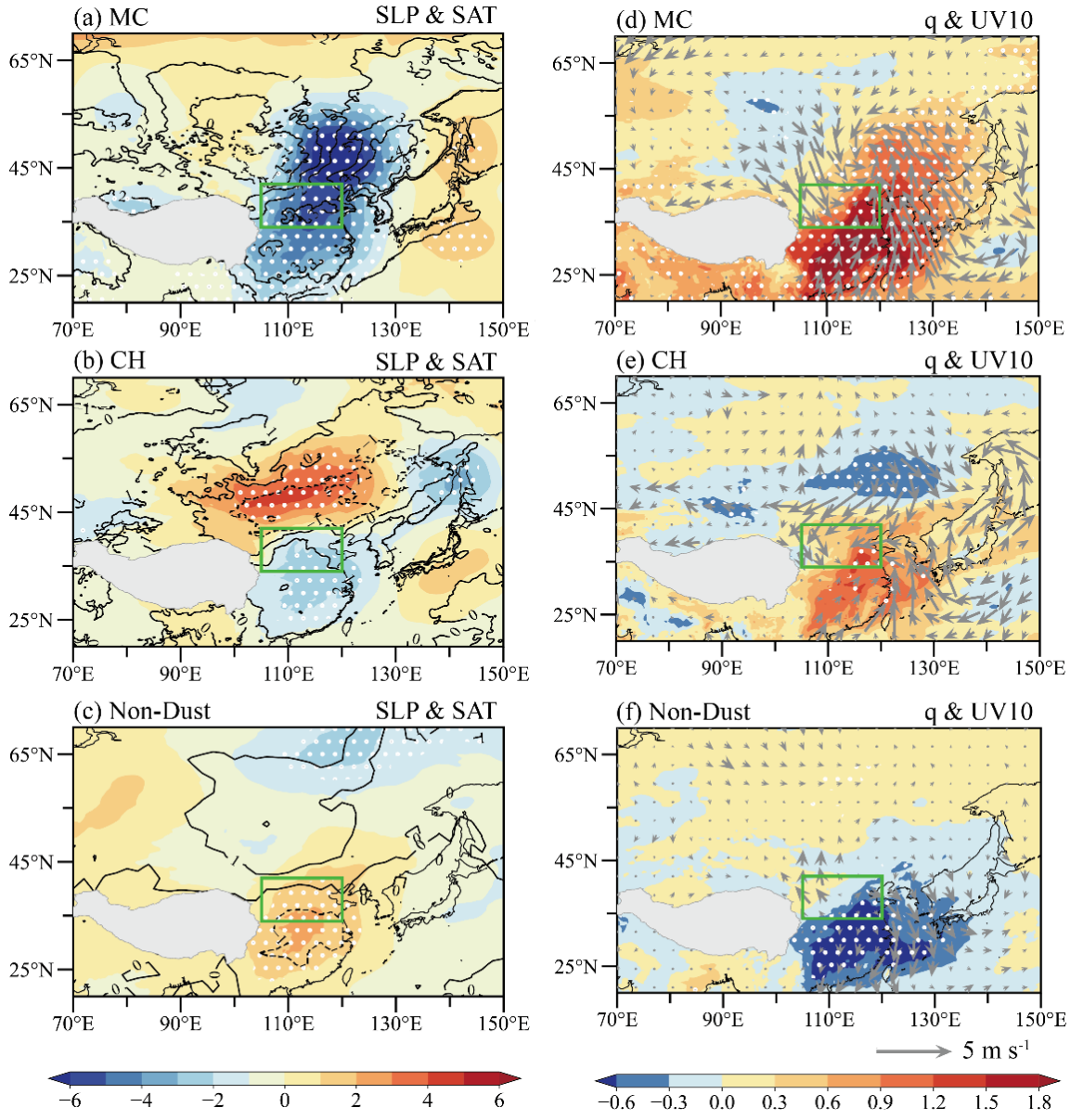

Figure 2. (a) Composite anomalies of SLP (shading, units: hPa) and SAT (contour, units: K) during MC days. White dots indicate that SLP anomalies exceed the 95% confidence level. Panel (b) and (c) are the same as panel (a) but for CH days and Non-Dust days. (d) Composite anomalies of q (shading, units: 10^{-3} kg kg^{-1}) and UV10 (vectors, units: m s^{-1}) during MC days. White dots indicate that q anomalies exceed the 95% confidence level. Panel (e) and (f) are the same as panel (d) but for CH days and Non-Dust days. The green boxes in panel (a)–(f) represent NC.

~~In the mid-troposphere, both the MC type and CH type exhibited cyclonic anomalies located to the northwest of NC, with noticeable anticyclonic anomalies to the southeast (Fig. 2a, b). The convergence of anomalous warm and cold air masses~~

brought about by these cyclonic and anticyclonic anomalies in mid-latitudes led to an increase in atmospheric baroclinicity, favoring the strengthening of westerlies (Fig. 2a, b). Compared to the CH type, the cyclonic anomaly associated with the MC type was stronger and more pronounced, extending further northwestward (Fig. 2a, b). Differences in the intensity of the 500 hPa cyclonic anomalies resulted in distinct configurations of surface synoptic systems. When the 500 hPa cyclonic anomalies were stronger, as seen during MC days, the surface Mongolian cyclone dominated (Fig. S1c). This enhanced the meridional circulation and set up a west-east orientation of the high and low-pressure systems as well as anomalies. (Fig. 3a). In contrast, for the CH days, weaker 500 hPa cyclonic anomalies led to a dominant cold high on the surface level (Fig. S1d). The meridional circulation weakened and a northwest-southeast orientation of the high and low-pressure systems as well as anomalies was set up (Fig. 3b).

The differences in system configurations could impact meteorological conditions near the surface. The pressure gradient between high and low-pressure systems led to strong gust winds near the surface on Dust days, with the Gust10 being stronger for the MC type compared to the CH type (Fig. S4a, b). The increase in the VATD, favoring atmospheric thermodynamic instability over NC and the dust source area (Fig. S4a, b). The enhanced surface wind speeds and thermodynamic instability in the dust source area increased the turbulence intensity in the atmospheric boundary layer (Garratt, 1992). The anomalously intensified turbulence aided in entraining surface dust particles into the atmosphere (Wiggs, 2011), while also raising the PBLH over the dust source area (Fig. S4c, d). The higher PBLH provided favorable conditions for the outward dispersion of dust particles in the air (Shao, 2008). It was observed that over the dust source area on MC and CH days, there was an anomalous divergence (Fig. 3d, e). Under the influence of anomalous northerly winds, dust particles were transported from the dust source area to NC, leading to an increase in PM10 concentrations (Fig. 3d, e). Divergent winds not only transported dust particles outward but also inhibited the inward transport of moisture into the dust source area. This resulted in relatively dry conditions near the surface in the dust source area, favoring dust emissions (Fig. 3d, e).

In addition to horizontal circulation, vertical circulation also played a crucial role in the generation of dust weather in NC. During Dust days, the cyclonic anomaly at 500 hPa exhibited an asymmetric vertical structure (Fig. 2d, e). On MC days, it was evident that the western ω at 500 hPa showed positive anomalies, while the eastern ω exhibited negative anomalies (Fig. 2d). The anomalous subsidence extended from the upper troposphere to the surface, transporting the westerly momentum from the upper troposphere down to the near-surface layer (Fig. 4a), resulting in stronger V850 and Gust10 (Fig. S4a, c). With the strengthening of the westerly momentum exchange, the conversion of kinetic energy from the mean flow to turbulence was enhanced (Liu and Liu, 2011). Furthermore, the anomalous subsidence also transported dry and cold air from the middle troposphere down to the near-surface layer (Fig. 4d). The intrusion of cold air favored the disruption of the stable boundary layer, leading to atmospheric thermal instability and an increase in turbulent kinetic energy (Liu and Liu, 2011). Stronger turbulence not only lifted surface dust but also resulted in higher PBLH. Under the influence of anomalous divergence in the lower troposphere, dust particles dispersed outward (Fig. 4d). The anomalous convergence zone in the eastern region facilitated the aggregation of dust particles and transported them to higher altitudes through anomalous upward motion. This prolonged the settling time of dust particles and facilitated their long-distance transport.

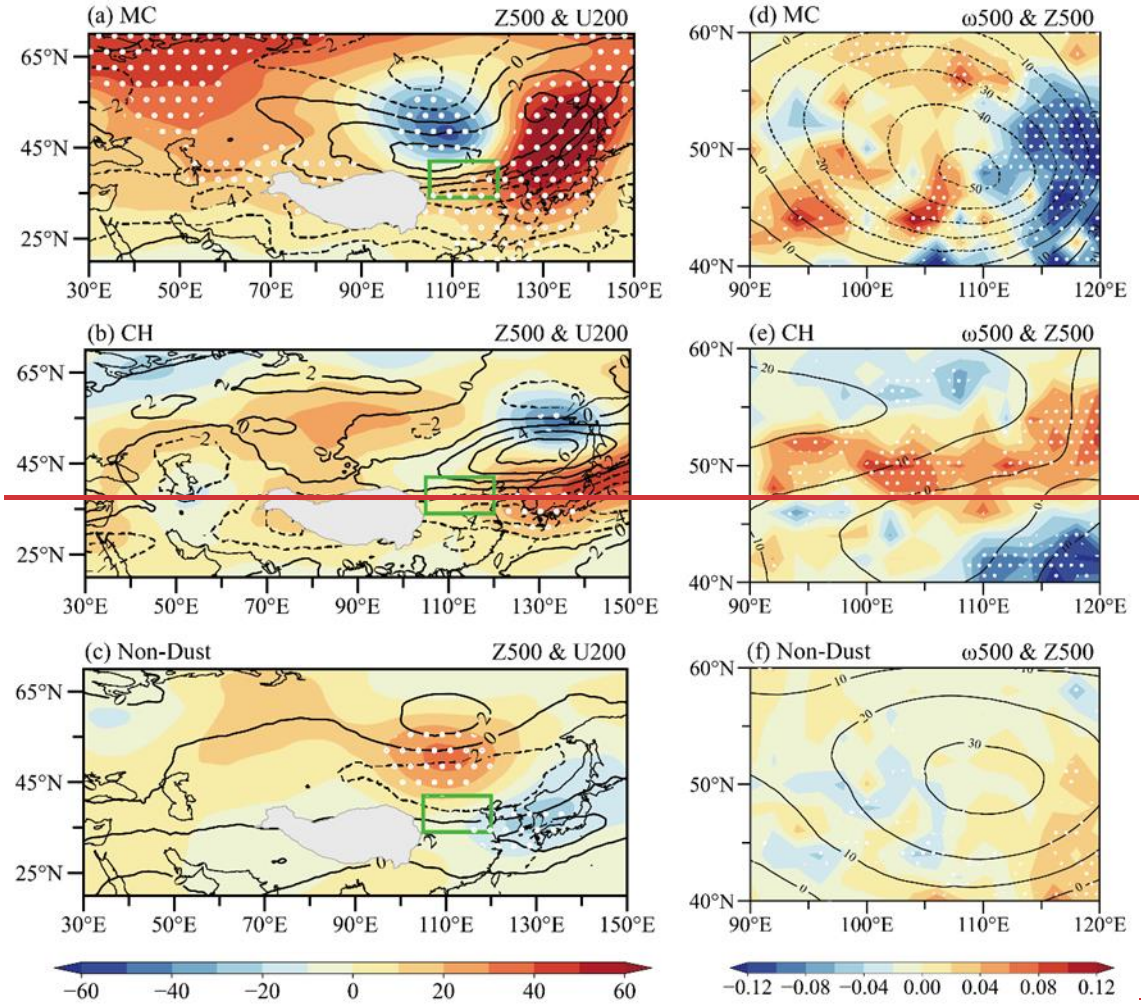

Figure 2. (a) Composite anomalies of Z500 (shading, units: geopotential meter, gpm) and U200 (contour, units: m s^{-1}) during MC days. White dots indicate that Z500 anomalies exceed the 95% confidence level. Panel (b) and (c) are the same as panel (a) but for CH days and Non-Dust days. (d) Composite anomalies of ω500 (shading, units: Pa s^{-1}) and Z500 (contour, units: gpm) during MC days. White dots indicate that ω500 anomalies exceed the 95% confidence level. Panel (e) and (f) are the same as panel (d) but for CH days and Non-Dust days. The green boxes in panel (a)–(f) represent NC.

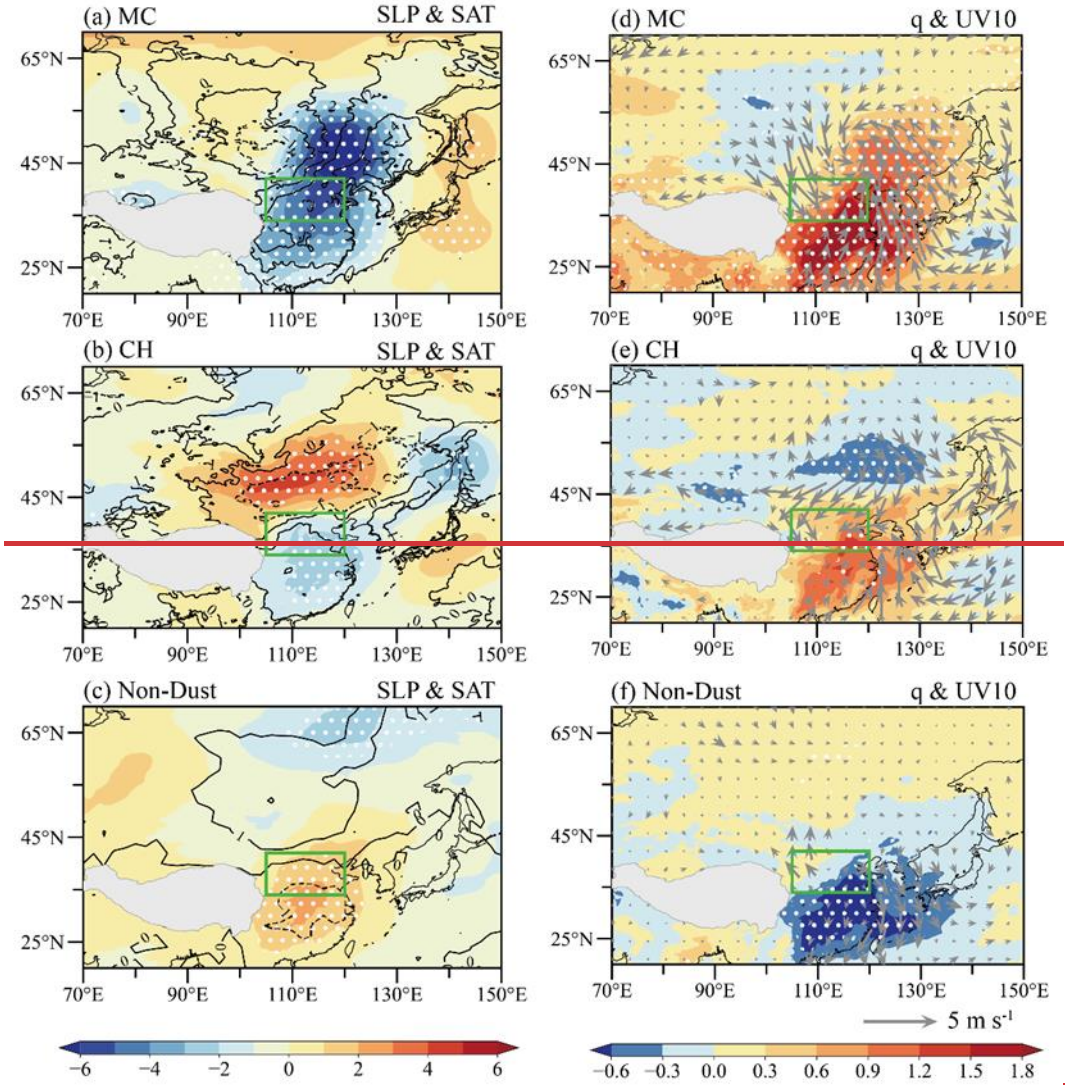

Figure 3. (a) Composite anomalies of SLP (shading, units: hPa) and SAT (contour, units: K) during MC days. White dots indicate that SLP anomalies exceed the 95% confidence level. Panel (b) and (c) are the same as panel (a) but for CH days and Non-Dust days. (d) Composite anomalies of q (shading, units: 10^{-3} kg kg^{-1}) and UV10 (vectors, units: m s^{-1}) during MC days. White dots indicate that q anomalies exceed the 95% confidence level. Panel (e) and (f) are the same as panel (d) but for CH days and Non-Dust days. The green

~~boxes in panel (a)–(f) represent NC.~~

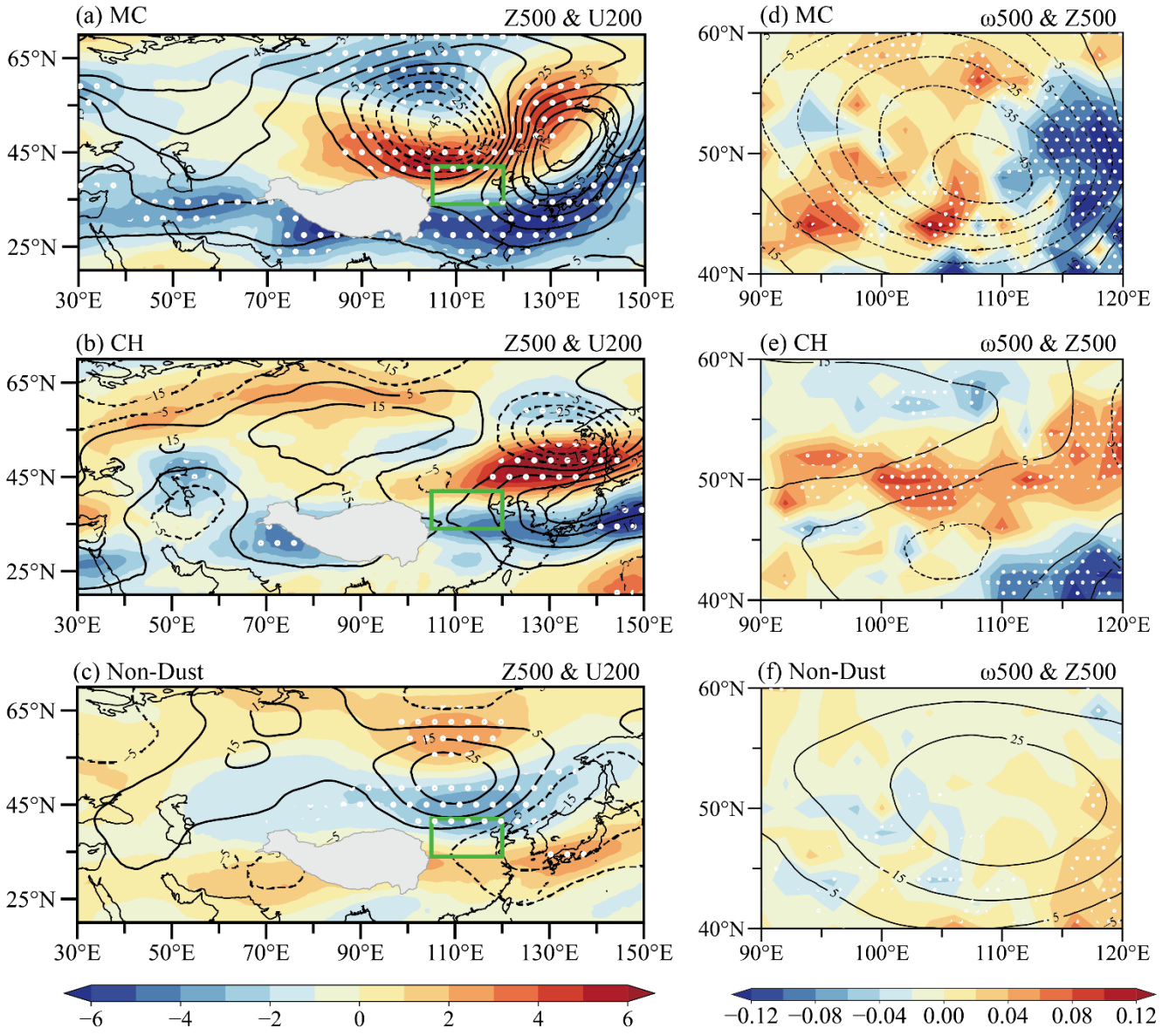

Figure 3. (a) Composite anomalies of Z500 (contour, units: geopotential meter, gpm) and U200 (shading, units: m s^{-1}) during MC days. White dots indicate that U200 anomalies exceed the 95% confidence level. Panel (b) and (c) are the same as panel (a) but for CH days and Non-Dust days. The green boxes in panel (a)–(c) represent NC. (d) Composite anomalies of ω500 (shading, units: Pa s^{-1}) and Z500 (contour, units: gpm) during MC days. White dots indicate that ω500 anomalies exceed the 95% confidence level. Panel (e) and (f) are the same as panel (d) but for CH days and Non-Dust days.

~~The latitudinal contrast of the CH type anomalous vertical circulation was weaker than that of the MC type (Fig. 4b, e), and the 500 hPa vertical velocity anomaly exhibited a northwest-southeast distribution pattern (Fig. 2e). The enhanced anomalous meridional vertical circulation increased the importance of the dust source area in the northward direction outside NC (Fig S5). The vegetation coverage in the northerly direction was relatively better than that in the northwesterly direction in the dust source area (Fig. S3a), leading to lower PM_{10} concentrations in NC under the influence of the CH type compared to the MC type. Overall, the meteorological variables on CH days exhibited spatial distribution characteristic similar to MC days but with weaker intensity. These results partially explained why PM_{10} concentrations were relatively lower on CH days compared to MC days.~~

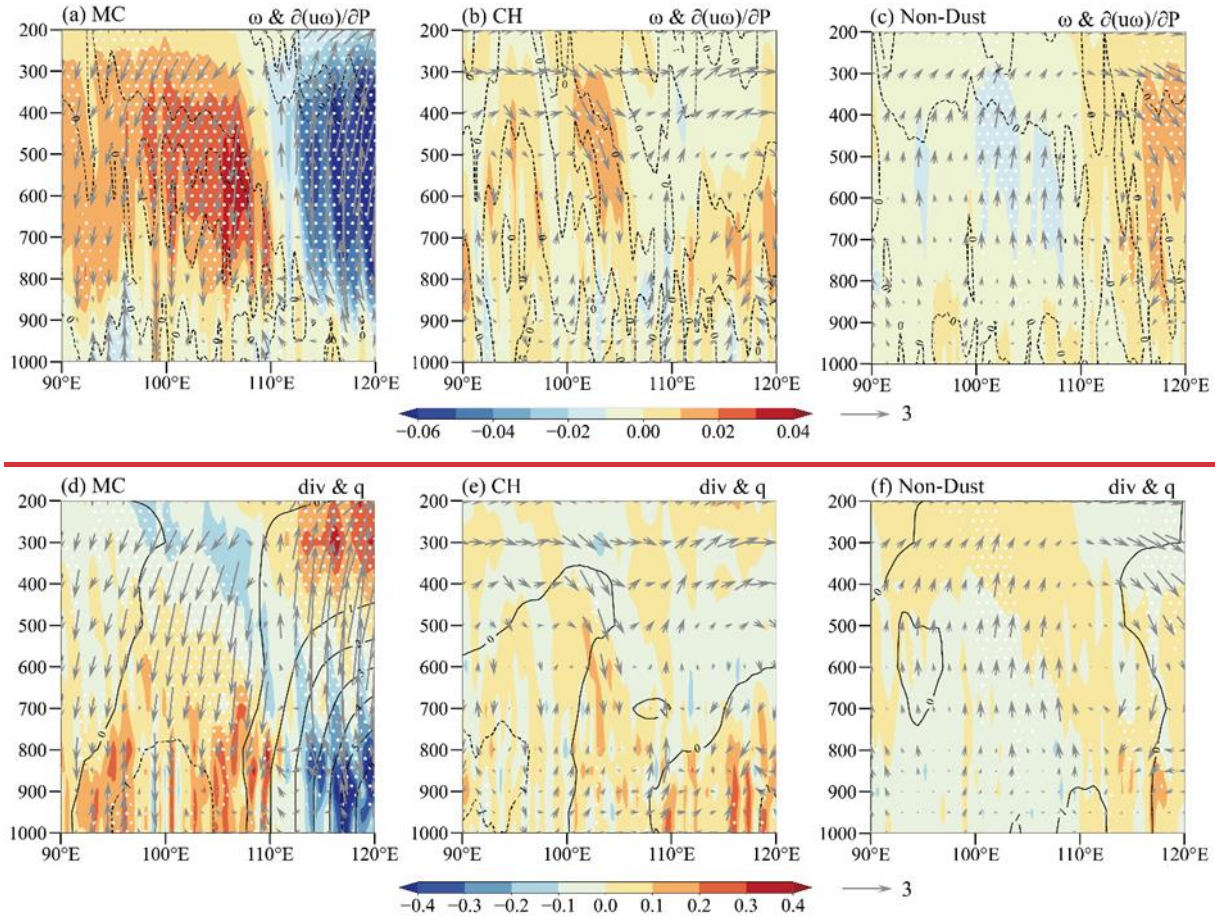
(a) MC
ω & ∂(uω)/∂P
(b) CH
ω & ∂(uω)/∂P
(c) Non-Dust
ω & ∂(uω)/∂P
200
300
400
500
600
700
800
900
1000
90°E
100°E
110°E
120°E
−0.06
−0.04
−0.02
0.00
0.02
0.04
3
(d) MC
div & q
(e) CH
div & q
(f) Non-Dust
div & q
−0.4
−0.3
−0.2
−0.1
0.0
0.1
0.2
0.3
0.4
3

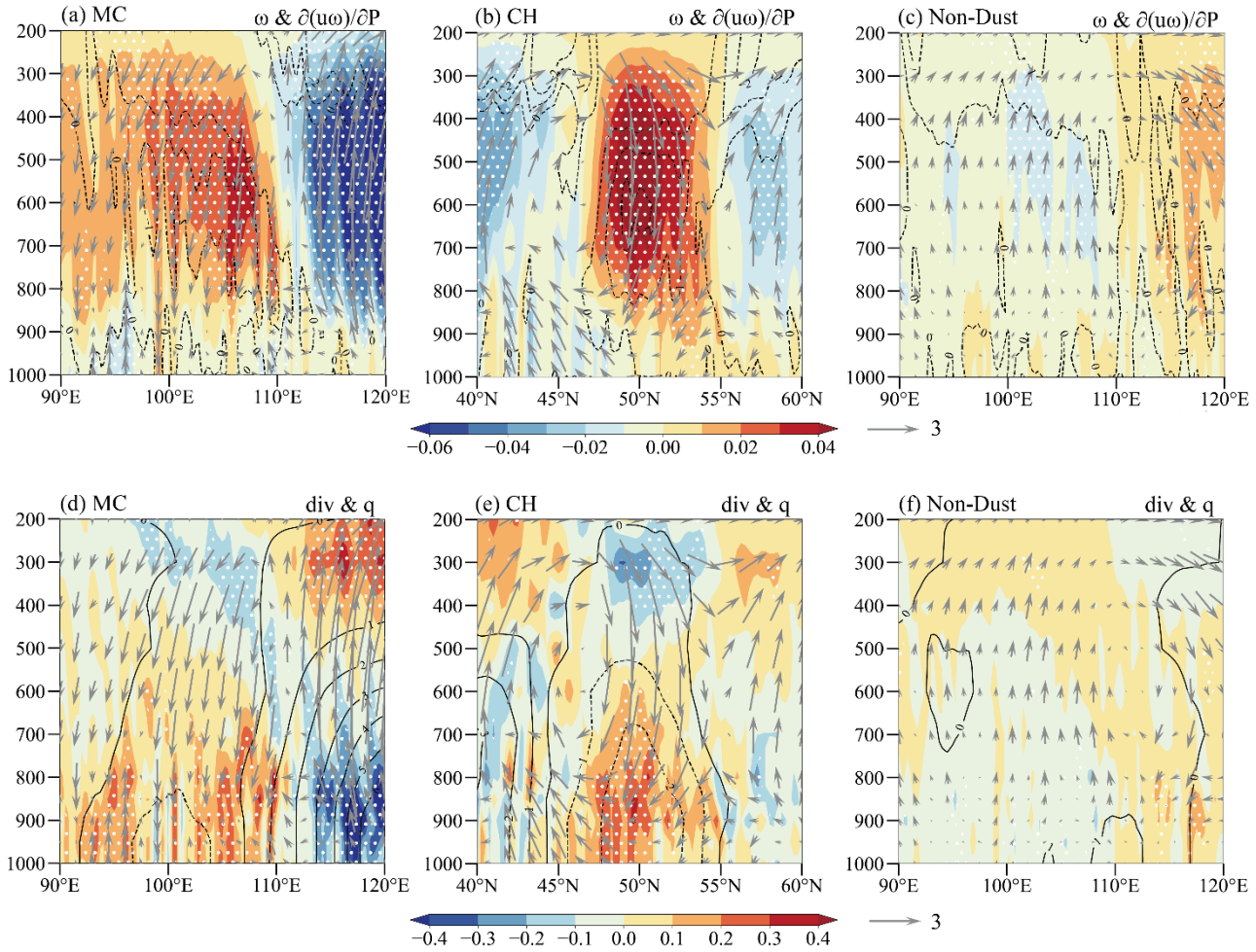

Figure 4. Composite anomalies of zonal component of the vertical circulation average over 40–60°N, 90–120°E during MC days: (a) The variables include ω (shading, units: Pa s^{-1}) and downward transport of westerly momentum (<0, dashed contour, units: 10^{-3} m s^{-2}). White dots indicate that ω anomalies exceed the 95% confidence level. The vectors represent ω (magnified 100 times) and zonal wind. (d) The variables include divergence (shading, units: 10^{-5} s^{-1}) and q (contour, units: 10^{-4} kg kg^{-1}). White dots indicate that divergence anomalies exceed the 95% confidence level. The vectors represent ω (magnified 100 times) and zonal wind. Panel (c) and (f) are the same as panel (a) and (d) respectively, but for Non-Dust days. Composite anomalies of meridional component of the vertical circulation average over 40–60° N, 90–120° E during CH days: (b) The variables include ω (shading, units: Pa s^{-1}) and downward transport of westerly momentum (<0, dashed contour, units: 10^{-3} m s^{-2}). White dots indicate that ω anomalies exceed the 95% confidence level. The vectors represent ω (magnified 100 times) and meridional wind. (e) The variables include divergence (shading, units: 10^{-5} s^{-1}) and q (contour, units: 10^{-4} kg kg^{-1}). White dots indicate that divergence anomalies exceed the 95% confidence level. The vectors represent ω (magnified 100 times) and meridional wind. ~~(a) Composite anomalies of zonal component of the vertical circulation average over 40–60°N, 90–120°E during MC days. The variables include ω (shading, units: Pa s^{-1}) and downward transport of westerly momentum (<0, dashed contour, units: 10^{-3} m s^{-2}). White dots indicate that ω anomalies exceed the 95% confidence level. The vectors represent ω (magnified 100 times) and zonal wind. Panel (b)~~

~~and (c) are the same as panel (a) but for CH days and Non-Dust days. (d) Composite anomalies of zonal component of the vertical circulation average over 40–60°N, 90–120°E during MC days. The variables include divergence (shading, units: 10^{-5} s^{-1}) and q (contour, units: 10^{-4} kg kg^{-1}). White dots indicate that divergence anomalies exceed the 95% confidence level. The vectors represent ω (magnified 100 times) and zonal wind. Panel (e) and (f) are the same as panel (d) but for CH days and Non-Dust days.~~

~~For comparison, the atmospheric circulation and meteorological conditions on Non-Dust days were also analyzed. The atmospheric circulation anomalies on Non-Dust days exhibited distribution characteristics opposite to those on Dust days. In the middle troposphere, the anticyclonic and cyclonic anomalies impeded the southward movement of cold air and the northward movement of warm air (Fig. 2c). The atmospheric baroclinicity weakened leading to a negative anomaly in the westerly wind (Fig. 2c). The opposite surface circulation anomalies led to southerly wind anomalies (Fig. 3c, f), causing an increase in q in the dust source area (Fig. 3f). During Non-Dust days, there was an opposite vertical circulation characterized by anomalous upward motion in the western region and anomalous downward motion in the eastern region (Fig. 2f). The anomalous upward motion suppressed the downward momentum flux and the intrusion of dry and cold air from the upper levels (Fig. 4c, f). All the meteorological conditions on Non-Dust days were unfavorable for the occurrence of dust weather.~~

5 A common predictor for the two dust weather types

The analysis results in Section 4 indicate that the anomalous circulation patterns and meteorological conditions during MC days, CH days, and Non-Dust days exhibited a certain linear correlation with the maximum PM_{10} concentration in NC. It is also found that the 500hPa cyclonic anomaly (CA) may be a key anomalous circulation system influencing MC and CH types. In order to comprehensively predict dust weather of the MC and CH types, we defined a series of meteorological indices to explore the common anomalous circulation systems influencing these two dust weather types. We calculated indices by selecting regions with the most significant spatial correlation coefficients between meteorological variables and PM_{10} concentrations. These indices exhibited significant correlations with the maximum PM_{10} concentration in NC with confidence levels exceeding 99% (Table 1). The composite values of the meteorological indices before normalization also showed significant differences during MC days, CH days, and Non-Dust days (Fig. 5b–i), correlating with the composite PM_{10} concentrations of the three categories (Fig. 1a). The 500 hPa cyclonic anomaly (CA) and anticyclonic anomaly (ACA) circulation systems were represented by the 500 hPa geopotential height indices I_Z500c and I_Z500a (Table 1). While I_Z500c showed significant correlations with other related meteorological indices, it couldn't explain the anomalies in VATD and PBLH well on Dust days (Table 2). If only CA is considered, it may not be sufficient to provide the thermodynamic instability conditions for dust weather. When considering the role of ACA, it can be observed that I_Z500a exhibited a stronger correlation with VATD and PBLH, with correlation coefficients reaching 0.639 and 0.534, respectively (Table 2). However, ACA alone may not explain the anomalies in specific humidity (q) on Dust days effectively.

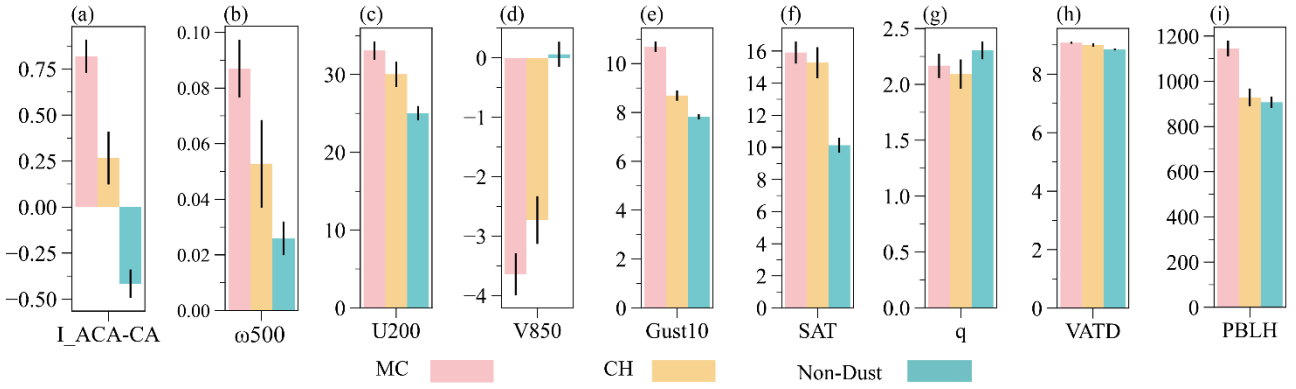

Figure 5. Composite meteorological index (a) I_ACA-CA, and composite meteorological variables (composite values of corresponding meteorological indices before normalization in Table 1): (b) ω500 (unit: Pa s^{-1}), (c) U200 (unit: m s^{-1}), (d) V850 (unit: m s^{-1}), (e) Gust10 (unit: m s^{-1}), (f) SAT (unit: K), (g) q (unit: kg kg^{-1}), (h) VATD (unit: K), (i) PBLH (unit: m) during MC days, CH days and Non-Dust days. The black error bars indicate the standard error.

By considering CA and ACA together, calculating the difference in Z500 between them and normalizing it, the index I_ACA-CA was defined. I_ACA-CA is significantly correlated with the maximum PM_{10} concentration in NC (R = 0.321), with an absolute correlation coefficient higher than I_Z500c (|R| = 0.205) and I_Z500a (|R| = 0.167). During MC days, CH days, and Non-Dust days, the composite values of I_ACA-CA also showed significant differences, corresponding to the composite PM_{10} concentration values during these days (Fig. 5a). Furthermore, I_ACA-CA exhibited significant correlations with meteorological conditions and horizontal circulation influencing dust weather in NC (Table 2), consistent with the physical mechanisms described in Section 4. Therefore, CA and ACA are closely related to dust weather in NC and are key anomalous circulation systems. I_ACA-CA is designated as a common predictor for the two types of Dust days in NC. Figure 6 displays the daily I_ACA-CA values in spring from 2015 to 2023, where positive I_ACA-CA captured 84.5% of MC days, 63.6% of CH days, and 76.5% of Dust days overall. All the Dust days in 2016 and 2023 were captured by I_ACA-CA (Fig. 6). In 2021, only one instance of lower PM_{10} concentration was not captured, with the rest being captured (Fig. 6). In correspondence with the positive I_ACA-CA observed two days, one day (I_ACA-CA>its one standard deviation), and zero day (I_ACA-CA>its one standard deviation) in advance, successful capture rates of 56.5%, 69.6%, and 76.5% for Dust days were achieved. These high percentages suggest that the reinforced positive I_ACA-CA significantly contributed to the high PM_{10} concentrations in NC.

Table 1. The definition of meteorological indices related to dust weather in NC and correlation coefficients (R) of observed daily maximum PM_{10} concentrations over NC with each index in spring from 2015 to 2023. All indices were the normalized area-averaged corresponding variables for their corresponding areas. All the correlation coefficients exceed the 99% confidence level.

Index	Definition	R
I_Z500c	Z500 over (44–52°N, 98–113°E)	-0.205

I_Z500a	Z500 over (33–40°N, 123–137°E)	0.167
I_ω500	ω500 over (42–48°N, 97–107°E)	0.157
I_U200	U200 over (40–45°N, 100–115°E)	0.220
I_V850	V850 over (38–46°N, 102–110°E)	-0.270
I_Gust10	Gust10 over (37–49°N, 103–118°E)	0.355
I_SAT	SAT over (23–33°N, 105–120°E) minus SAT over (43–50°N, 100–110°E)	0.383
I_q	q over (45–53°N, 91–103°E)	-0.171
I_VATD	VATD over (42–47°N, 106–116°E)	0.118
I_PBLH	PBLH over (46–55°N, 100–110°E)	0.126
I_ACA-CA	Z500 over (33–40°N, 123–137°E) minus Z500 over (44–52°N, 98–113°E)	0.321

The evolution of CA, ACA and related atmospheric circulation anomalies before MC days and CH days was further investigated (Fig. 7). Prior to both types of Dust days, CA and ACA moved eastward towards NC (Fig. 7). For MC type, CA and ACA from western Siberia and Lake Baikal gradually strengthened as they moved eastward (Fig. 7a–d). The development of the Mongolian cyclone intensified (Fig. S7a–d), accompanied by an eastward strengthening of the associated surface low-pressure anomaly and cyclonic winds to the northwest of NC (Fig. 7a–c). As the surface low pressure anomaly moved eastward, the anomalous southerly winds north of NC shifted to anomalous northerly winds (Fig. 7c, d). The actual wind directions changed from westerly to northwesterly (Fig. S7c, d). For CH type, CA and ACA were relatively positioned more to the east (Fig. 7e), with CA moving eastward from central Siberia and gradually weakening, while ACA moving eastward from Northeast Asia gradually strengthened (Fig. 7e–h). The cold high intensified as it moved eastward (Fig. S7e–g), accompanied by an eastward strengthening of the surface high-pressure anomaly (Fig. 7e–g). One day before the CH-type dust day, the surface high-pressure anomaly replaced the low-pressure anomaly to the north of NC (Fig. 7g, h), and the wind anomalies north of NC shifted from southwest to northeast (Fig. 7f–h). The actual wind directions changed from westerly to northerly directions (Fig. S7f–h). In summary, the development and movement of CA and ACA aligned with the occurrence and development of MC days and CH days in NC. The common predictor I_ACA-CA served as a meaningful indicator for predicting dust weather in NC.

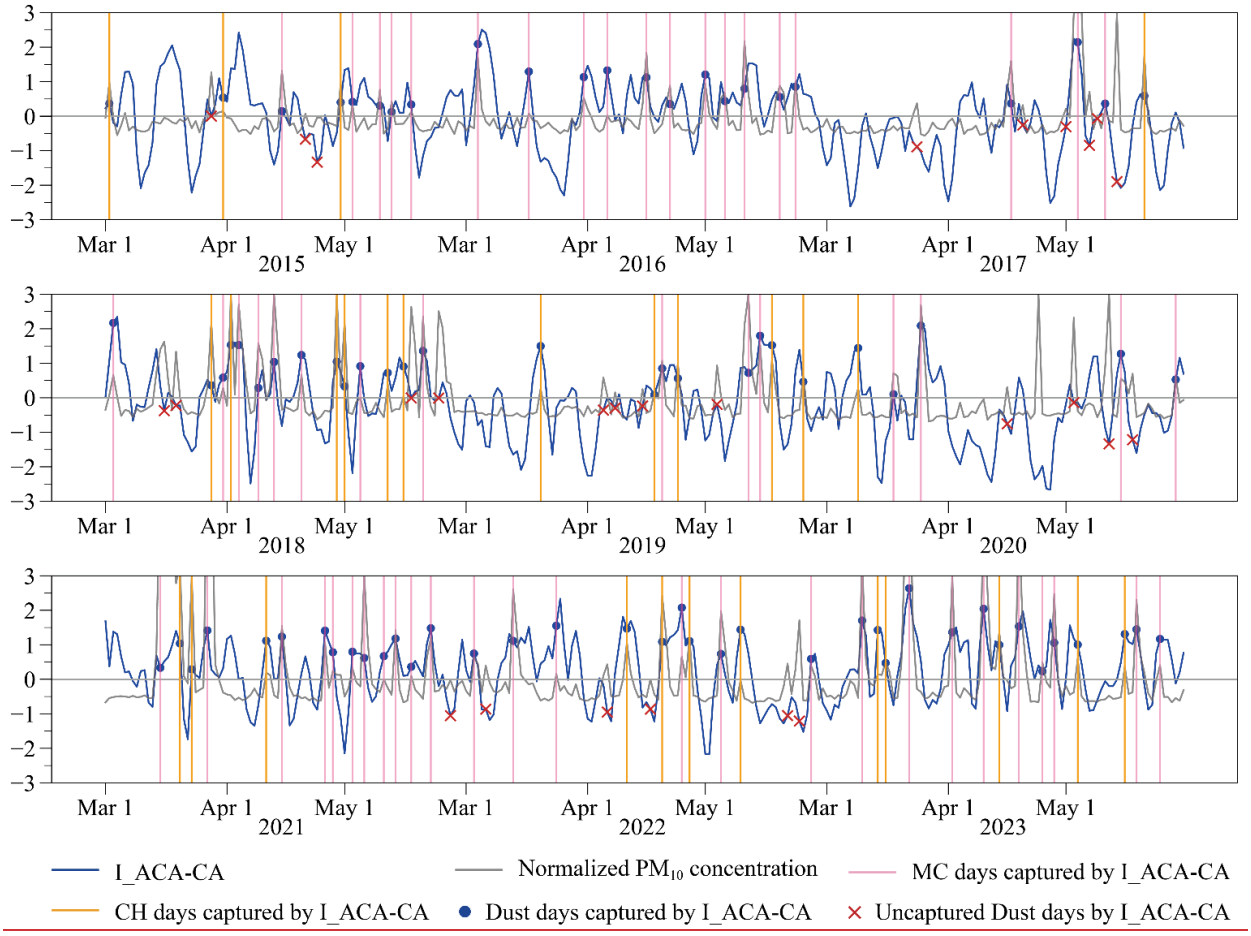

Figure 6. Daily I_ACA-CA (blue line) and normalized daily maximum PM_{10} concentrations observed in NC (grey line) in March (Mar), April (Apr) and May from 2015 to 2023. The blue dots indicate the Dust days captured when I_ACA-CA>0 and the corresponding I_ACA-CA value. The pink and yellow vertical lines indicate the MC days and CH days captured when I_ACA-CA>0, respectively. The red "x" marks represent the Dust days that I_ACA-CA failed to capture.

~~**Table 1.** The definition of meteorological indices related to dust weather in NC and correlation coefficients (R) of observed daily maximum PM_{10} concentrations over NC with each index in spring from 2015 to 2023. All indices were the normalized area-averaged corresponding variables for their corresponding areas. All the correlation coefficients exceed the 99% confidence level.~~

~~Index~~	~~Definition~~	~~R~~
~~I_Z500c~~	~~Z500 over (44–52°N, 98–113°E)~~	~~-0.205~~
~~I_Z500a~~	~~Z500 over (33–40°N, 123–137°E)~~	~~0.167~~
~~I_ω500~~	~~ω500 over (42–48°N, 97–107°E)~~	~~0.157~~
~~I_U200~~	~~U200 over (40–45°N, 100–115°E)~~	~~0.220~~
~~I_V850~~	~~V850 over (38–46°N, 102–110°E)~~	~~-0.270~~

I_Gust10	Gust10 over (37–49°N, 103–118°E)	0.355
I_SAT	SAT over (23–33°N, 105–120°E) minus SAT over (43–50°N, 100–110°E)	0.383
I_q	q over (45–53°N, 91–103°E)	-0.171
I_VATD	VATD over (42–47°N, 106–116°E)	0.118
I_PBLH	PBLH over (46–55°N, 100–110°E)	0.126
I_ACA_CA	Z500 over (33–40°N, 123–137°E) minus Z500 over (44–52°N, 98–113°E)	0.321

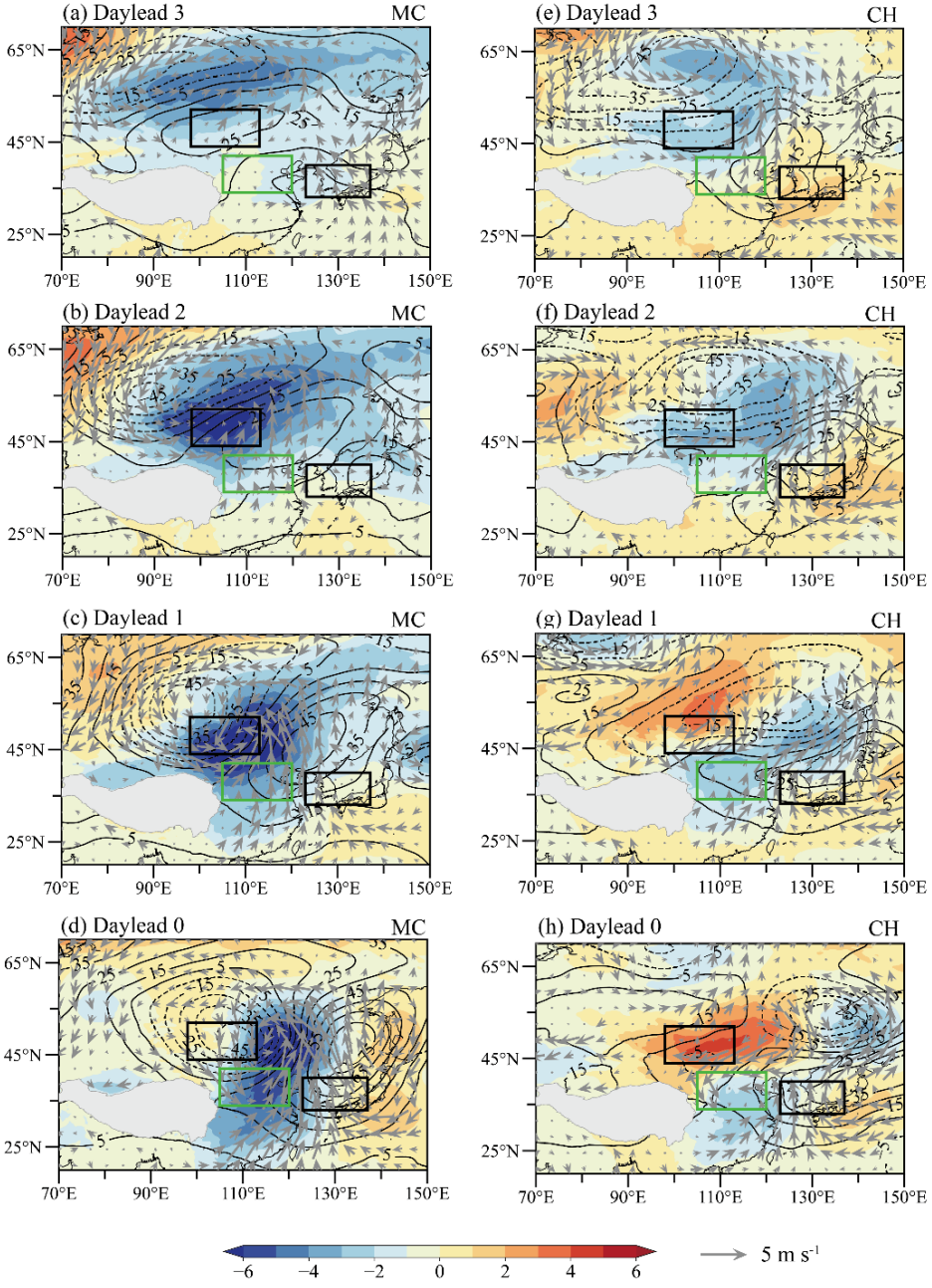

Figure 7. (a)–(d) Lead composite evolution of Z500 (contour, unit: gpm) anomalies, SLP (shading, unit: hPa) anomalies, and UV850 (vectors, units: m s^{-1}) anomalies during MC days. Panel (e)–(h) are the same as panel (a)–(d) but for CH days. The green boxes in panel (a)–(h) represent NC, while the black boxes represent the region for calculating I_ACA-CA.

Table 2. The correlation coefficients of I_Z500c, I_Z500a and I_ACA-CA with other meteorological indices (Table 1) in spring from 2015 to 2023. All the correlation coefficients exceed the 99% confidence level. The symbol "—" denotes that the correlation coefficient is not statistically significant and therefore has been excluded from the analysis.

Index	I_Gust10	I_VATD	I_PBLH	I_SAT	I_q	I_ω500	I_U200	I_V850
I_Z500c	-0.216	0.500	0.191	-0.462	0.693	-0.130	-0.470	0.195
I_Z500a	0.256	0.639	0.534	0.292	0.367	—	0.269	-0.117
I_ACA-CA	0.407	0.113	0.292	0.652	-0.287	—	0.638	-0.269

~~Based on the results of Sect. 4, correlations between meteorological conditions and the daily maximum PM_{10} concentration in NC can be observed. To further confirm the relationship, the spatial correlation coefficients were calculated (Fig. S6). Significant correlation coefficients between meteorological conditions and PM_{10} concentration further confirmed the aforementioned results (Fig. S6). The increased meridional temperature differences reflected the enhanced atmospheric baroclinicity in mid-latitude regions (Fig. S6f; Zhang et al., 2021), which provided favorable conditions for the generation of surface synoptic systems and strong wind anomalies. In the selected regions with significant correlations, corresponding meteorological indices were defined, and the correlation coefficients between the daily maximum PM_{10} concentration in NC were calculated (Table 1). All correlation coefficients passed a significance test at the 99% level ($p<0.01$). By examining the area-averaged meteorological variables in the regions of significant correlation, it was also found that the meteorological conditions on MC days, CH days as well as Non-Dust days, exhibited significant differences and had certain correlations with the PM_{10} concentration (Fig. 5b–i). Specifically, the meteorological conditions favoring dust weather in the MC type were stronger than those in the CH type, leading to higher PM_{10} concentrations on MC days compared to CH days, making extreme dust events more likely to occur on MC days.~~

~~As described in Sect. 4, the 500 hPa cyclonic anomaly affected near-surface meteorological conditions through the associated vertical and horizontal circulation anomalies, leading to dust weather in NC. By correlation analysis, it was found that there was a significant relationship between 500 hPa cyclonic anomaly (I_Z500c) and the related meteorological condition indices (Table 2). This confirmed the physical mechanisms outlined in Sect. 4. However, based on the correlation coefficient results, 500 hPa cyclonic anomaly (I_Z500c) alone did not explain the anomalies in VATD and PBLH well (Table 2). At the 500 hPa level, there was also an anticyclonic anomaly that showed a significant correlation with the PM_{10} concentration in NC (Fig. S6a). This anomaly provides warm air advection disturbances in the mid-latitudes on Dust days. Therefore, an analysis of its relationship with near-surface meteorological conditions was warranted. The correlation coefficients between the anticyclonic anomaly (I_Z500a) and the near-surface meteorological indices all passed a significance test at the 99% level (Table 2). The strongest positive correlations were observed between I_Z500a and both I_VATD and I_PBLH, with correlation coefficients reaching 0.639 and 0.534, respectively (Table 2).~~

~~**Table 1.** The definition of meteorological indices related to dust weather in NC and correlation coefficients (R) of observed daily maximum PM_{10} concentrations over NC with each index in spring from 2015 to 2023. All indices were the normalized area-averaged corresponding variables for their corresponding areas. All the correlation coefficients exceed the 99% confidence level.~~

Index	Definition	R
I_Z500c	Z500 over (44–52°N, 98–113°E)	-0.205
I_Z500a	Z500 over (33–40°N, 123–137°E)	0.167
I_ω500	ω500 over (42–48°N, 97–107°E)	0.157
I_U200	U200 over (40–45°N, 100–115°E)	0.220
I_V850	V850 over (38–46°N, 102–110°E)	-0.270
I_Gust10	Gust10 over (37–49°N, 103–118°E)	0.355
I_SAT	SAT over (23–33°N, 105–120°E) minus SAT over (43–50°N, 100–110°E)	0.383
I_q	q over (45–53°N, 91–103°E)	-0.171
I_VATD	VATD over (42–47°N, 106–116°E)	0.118
I_PBLH	PBLH over (46–55°N, 100–110°E)	0.126
I_ACA-CA	Z500 over (33–40°N, 123–137°E) minus Z500 over (44–52°N, 98–113°E)	0.321

Table 2. The correlation coefficients of I_Z500c, I_Z500a and I_ACA-CA with other meteorological indices (Table 1) in spring from 2015 to 2023. All the correlation coefficients exceed the 99% confidence level. The symbol "—" denotes that the correlation coefficient is not statistically significant and therefore has been excluded from the analysis.

Index	I_Gust10	I_VATD	I_PBLH	I_SAT	I_q	I_ω500	I_U200	I_V850
I_Z500c	-0.216	0.500	0.191	-0.462	0.693	-0.130	-0.470	0.195
I_Z500a	0.256	0.639	0.534	0.292	0.367	—	0.269	-0.117
I_ACA-CA	0.407	0.113	0.292	0.652	-0.287	—	0.638	-0.269

The common circulation index I_ACA-CA of the two dust weather types was defined by calculating the difference in Z500 between the 500 hPa anticyclonic anomaly and cyclonic anomaly and normalizing it (Table 1). Significant differences in composite I_ACA-CA were observed for MC days, CH days, and Non-Dust days (Fig. 5a). These differences corresponded to the relationship with PM_{10} concentrations among the three types. I_ACA-CA exhibited significant correlations with PM_{10} concentrations, showing a correlation coefficient of 0.321, passing the 99% significance test ($p<0.01$). It also demonstrated correlations with near-surface meteorological indices and horizontal circulation indices (Table 2). These correlation coefficients effectively confirmed that the 500 hPa cyclonic and anticyclonic circulation anomalies influenced near-surface meteorological conditions through horizontal and vertical circulation. Figure 6 displays the daily I_ACA-CA values in spring from 2015 to 2023, where positive I_ACA-CA captured 83.6% of MC days, 63.6% of CH days, and 76.1% of Dust days overall. All the Dust days in 2016 and 2023 were captured by I_ACA-CA (Fig. 6). In 2021, only one instance of lower PM_{10} concentration was not captured, with the rest being captured (Fig. 6). In correspondence with the positive I_ACA-CA observed

~~two days, one day (I_ACA-CA>its one standard deviation), and zero day (I_ACA-CA>its one standard deviation) in advance, successful capture rates of 55.6%, 69.2%, and 76.1% for Dust days were achieved. These high percentages suggest that the reinforced positive I_ACA-CA significantly contributed to the high PM_{10} concentrations in NC. Thus, I_ACA-CA served as a meaningful indicator for forecasting dust weather in NC.~~

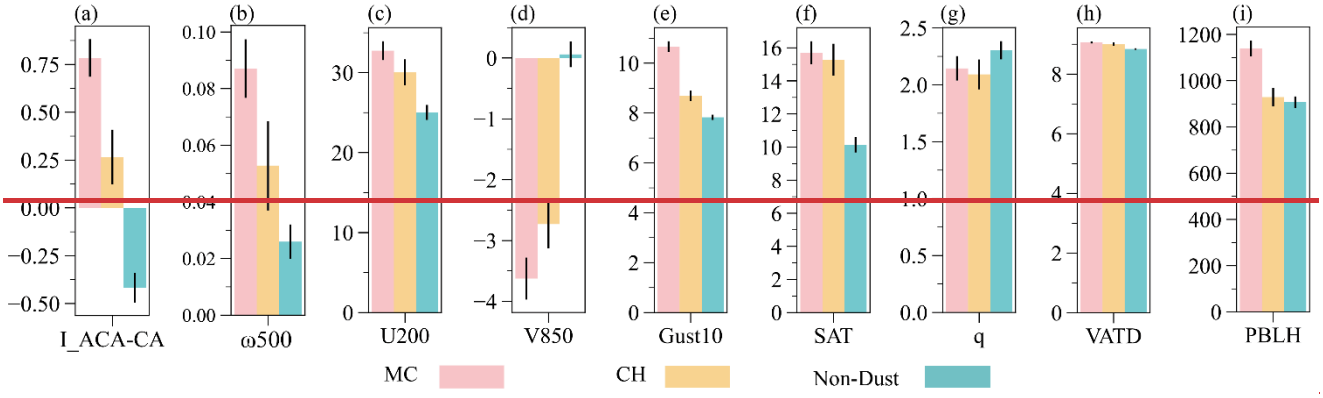

~~**Figure 5.** Composite meteorological index: (a) I_ACA-CA, and composite meteorological variables (composite values of corresponding meteorological indices before normalization in Table 1): (b) ω500 (unit: Pa s^{-1}), (c) U200 (unit: m s^{-1}), (d) V850 (unit: m s^{-1}), (e) Gust10 (unit: m s^{-1}), (f) SAT (unit: K), (g) q (unit: kg kg^{-1}), (h) VATD (unit: K), (i) PBLH (unit: m) during MC days, CH days and Non-Dust days. The black error bars indicate the standard error.~~

6 Conclusion and discussion

In recent years, the frequency and intensity of dust weather in NC have been increasing, with many adverse effects on human health, national economy, and ecological environment. This study selected Dust days based on PM_{10} concentrations in NC in spring from 2015 to 2023. By objectively identifying the presence of the Mongolian cyclone and based on the main surface synoptic systems, Dust days were classified into MC type (61.7%) and CH type (38.3%). The PM_{10} concentrations on MC days were higher and more extreme compared to those on CH days, with average PM_{10} concentrations at 3076 μg m^{-3} and 2391 μg m^{-3}. Figure 8 illustrates the three-dimensional atmospheric circulation anomalies structures and relevant dynamic processes of the two types of dust weather with distinct PM_{10} concentrations in NC. The 500 hPa cyclonic and anticyclonic circulation anomalies have been investigated to be correlated with both types of Dust days. In order to comprehensively forecast the two types of dust weather, a common predictor has been constructed based on the anomalous circulation systems at 500 hPa, providing insights for dust weather forecasting and climate prediction in NC.

This study differs from traditional weather classification studies by not further categorizing weather types beyond the Mongolian cyclone. The circulation anomalies related to the two types of dust weather were explored to identify the common predictor. The study designates the peak PM_{10} concentration during periods when the daily maximum PM_{10} concentration exceeds 1000 μg m^{-3} as Dust days, representing a typical dust event. This aims to capture the most significant circulation

anomalies and extreme conditions during dust events. The transitional phase during the development and cessation of dust weather in NC has not been included in this study. Previous studies have investigated the relationship between PM_{10} concentration thresholds and traditional dust weather levels, but a unified standard has not yet been established. According to the standards used in previous studies (Wan et al. 2004; Wang et al., 2008), Dust days identified by the 1000 μg m^{-3} PM_{10} concentration threshold primarily correspond to the traditional meteorological classifications of blowing dust, sand and dust storm, and severe sand and dust storm. Furthermore, dust weather identified by PM_{10} concentrations may differ from traditional dust weather defined based on visibility and other meteorological phenomena. For example, in the years 2015–2023, Dust days defined by PM_{10} concentrations were most frequent in May, rather than in April as seen in previous studies. However, the increase in the number of dust days in May may be a recent trend that requires further study.

The common predictor (I_ACA-CA) of the two dust weather types in NC was identified. The research findings demonstrated that the I_ACA-CA had good indicative significance for dust weather in NC. Previous studies have primarily focused on the role of Mongolian cyclones in North China's dust weather. However, in addition to Mongolian cyclones, systems like cold high can also lead to dust storms in North China. The common predictor offers a more comprehensive prediction for both types of dust weather compared to solely considering the Mongolian cyclone, capturing more dust days. The ability of the C3S seasonal forecast model to reproduce I_ACA-CA was further assessed. The I_ACA-CA calculated by ECMWF, DWD, and MF seasonal forecast models with a one-month lead captured around 50% of spring dust days when positive. These ratios are all lower than the capture rate of I_ACA-CA for dust weather (76.5%) calculated from ERA5 data, indicating the need for further improvement. It is worth noting that due to the lower spatial resolution (1°×1°) of the C3S model forecast data relative to the ERA5 data (0.25°×0.25°), the SLP produced by the C3S model failed to effectively identify the presence of the Mongolian cyclone. Therefore, the introduction of the common predictor (I_ACA-CA) is of great significance for dust weather prediction in NC. However, due to constraints imposed by PM_{10} concentration observation data, the study period only covered the years 2015 to 2023. Further research is needed to test the effectiveness of the I_ACA-CA indicator over longer time series and to utilize it for predicting future dust weather.

~~In recent years, the frequency and intensity of dust weather in NC have been increasing, with many adverse effects on human health, national economy, and ecological environment. This study selected Dust days based on PM_{10} concentrations in NC during spring from 2015 to 2023. By objectively identifying the presence of the Mongolian cyclone and based on the main surface synoptic systems, Dust days were classified into MC type (62.4%) and CH type (37.6%). The PM_{10} concentrations on MC days were higher and more extreme compared to those on CH days, with average PM_{10} concentrations at 3076 μg m^{-3} and 2391 μg m^{-3}. The research results indicate that the 500 hPa atmospheric circulation anomalies affect near surface meteorological conditions through related horizontal and vertical circulation, leading to different intensities of dust weather in NC. Figure 7 illustrates the three-dimensional atmospheric circulation anomalies structures and relevant dynamic processes of the two types of dust weather with distinct PM_{10} concentrations in NC. The different intensities of the 500 hPa cyclonic and anticyclonic anomalies led to differences in the configuration of surface systems. This was manifested as different meridional extents of circulation, with the meridional circulation of the MC type being greater than that of the CH type. This also resulted~

in differences in the intensity of near-surface meteorological factors, with the meteorological conditions for dust weather being more favorable for the MC type compared to the CH type. The strong gust winds and atmospheric thermal instability caused dust particles from the dust source areas to be lifted into the air, with the anomalous downward momentum in the upper troposphere exacerbating this process. Subsequently, under the influence of the anomalous northerly winds, dust particles were transported to NC, leading to an increase in PM_{10} concentrations, with the PM_{10} concentration on MC days higher than that on CH days.

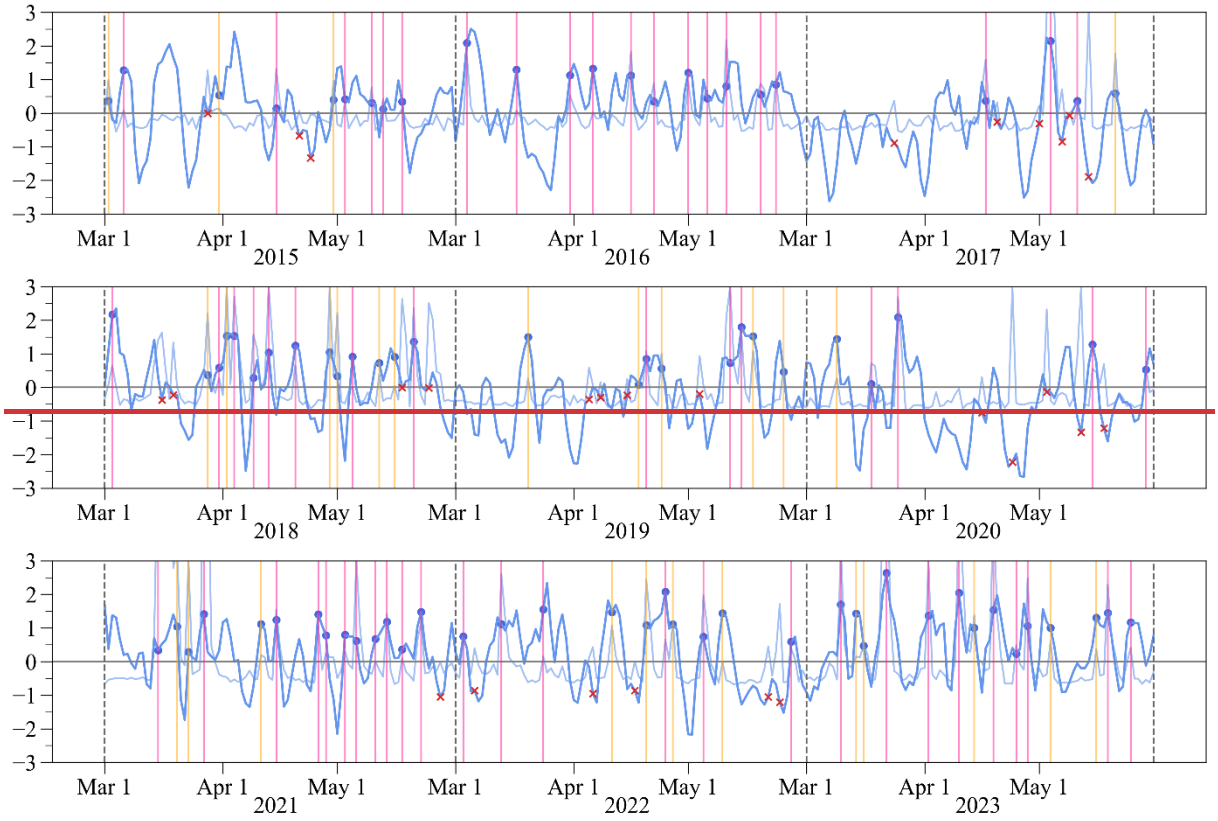

Figure 6. Daily I_ACA-CA (blue line) and normalized daily maximum PM_{10} concentrations observed in NC (light blue line) in March (Mar), April (Apr) and May from 2015 to 2023. The blue dots indicate the Dust days captured when I_ACA-CA>0 and the corresponding I_ACA-CA value. The pink and orange vertical lines indicate the MC days and CH days captured when I_ACA-CA>0, respectively. The red "x" marks represent the Dust days that I_ACA-CA failed to capture. The gray vertical dashed lines separate each year.

The common predictor (I_ACA-CA) of the two dust weather types in NC was identified. The research findings demonstrated that the I_ACA-CA had good indicative significance for dust weather in NC. The ability of the C3S model (ECMWF SEAS5.1) to reproduce I_ACA-CA was further assessed. The I_ACA-CA calculated by C3S data with a one-month lead captured 47.0% of spring Dust days when positive. The relative error compared to the capture rate (76.1%) of I_ACA-CA calculated by ERA5 data was 38.2%. The I_ACA-CA calculated from C3S model forecast data has a lower capture rate

~~for dust weather and exhibits errors compared to ERA5, indicating the need for further improvement. It is worth noting that due to the lower spatial resolution (1°×1°) of the C3S model forecast data relative to the ERA5 data (0.25°×0.25°), the SLP produced by the C3S model failed to effectively identify the presence of the Mongolian cyclone. Therefore, the introduction of the common predictor (I_ACA-CA) is of great significance for dust weather prediction in NC. However, due to constraints imposed by PM_{10} concentration observation data, the study period only covered the years 2015 to 2023. Further research is needed to test the effectiveness of the I_ACA-CA indicator over longer time series and to utilize it for predicting future dust weather. The study solely considered the impact of dynamic factors on dust weather. While the dust source condition also plays a crucial role in the formation of dust weather. Previous research by Yin et al. (2022) found that climate accumulation effects could influence the dust source conditions for spring dust weather, thereby regulating its intensity. For the "3.15" super dust storm in 2021, although the I_ACA-CA exhibited a certain level of positive signal, it did not indicate the extremity of the dust weather event (Fig. 6). For the severe dust storm on March 22 2023, the I_ACA-CA indicator performed well, showing the extreme characteristics in intensity (Fig. 6). The deviation in indicating extreme dust storm intensity by I_ACA-CA may be due to the lack of consideration of dust source conditions. Therefore, the development of a dust weather prediction model that comprehensively considers the synergistic effects of dust source conditions and dynamic factors awaits further research.~~

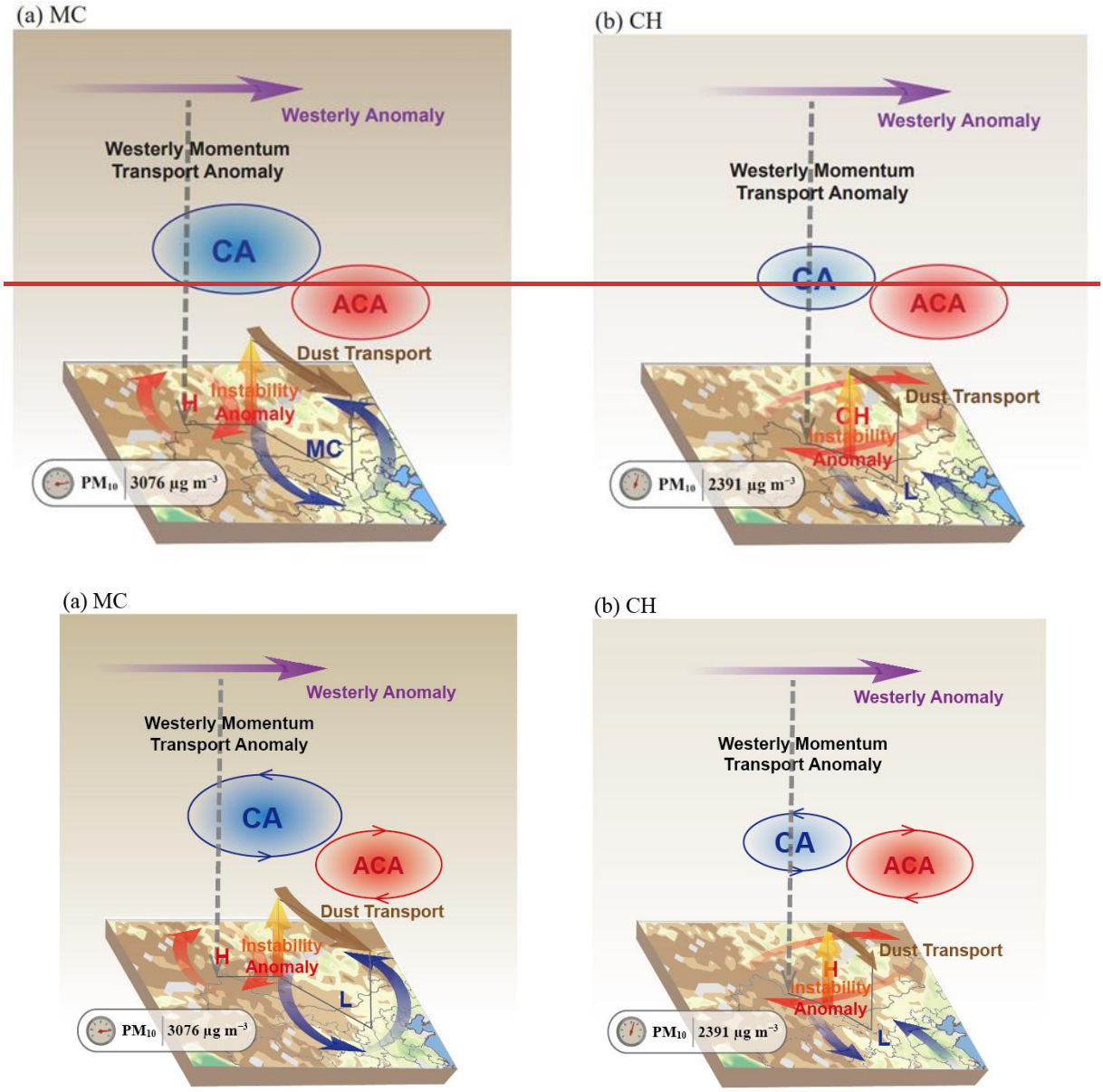

Figure ~~7~~8. Schematic diagram for the three-dimensional atmospheric circulation anomalies and related dynamic processes of (a) MC type and (b) CH type dust weather with distinct PM_{10} concentrations in NC. 500 hPa cyclonic anomaly (CA) and anticyclonic anomaly (ACA) are the key anomalous circulation systems for the two types. ~~led to different configurations of anomalous circulation systems on the surface level.~~ "L" and "H" respectively represent surface low-pressure anomalies and high-pressure anomalies. The anomalous gust winds and thermal instability near the dust source area favored dust lifting. Enhanced 200 hPa westerly winds, with momentum transport downward, favored further increases in surface wind speeds. Anomalous northerly winds facilitated the emission and transport of~~ed~~ dust particles ~~southward affecting NC~~. The shading on the surface represents NDVI in March 2023. The directions of the arrows indicate anomalous airflow directions. The average PM_{10} concentrations of MC and CH days are demonstrated in the left bottom of each panel.

Data Availability.

Hourly PM_{10} concentration data was available at https://quotsoft.net/air/ (China National Environmental Monitoring Centre, 20232024). Hourly ERA5 reanalysis dataset was available at https://cds.climate.copernicus.eu/datasets/reanalysis-era5-pressure-levels?tab=downloadhttps://cds.climate.copernicus.eu/cdsapp#!/dataset/reanalysis-era5-pressure-levels?tab=overview (ERA5, 2024). The NDVI data could be acquired from https://www.ncei.noaa.gov/access/metadata/landing-page/bin/iso?id=gov.noaa.ncdc:C01558 (NOAA, 2023). The C3S seasonal forecast data was available at https://cds.climate.copernicus.eu/datasets/seasonal-original-single-levels?tab=downloadhttps://cds.climate.copernicus.eu/cdsapp#!/dataset/10.24381/cds.50ed0a73?tab=overview (C3S, 2024).

Authors' contribution

Yin Z. C. and Wang H. J. designed the research. Huo Q. Y., Ma X. Q. and Yin Z. C. performed the research. Huo Q. Y. prepared the manuscript with contributions from all co-authors.

Competing interests

The authors declare that they have no conflict of interest.

Acknowledgements

This work was supported by the National Natural Science Foundation of China (42088101).

References

Ahmadzai, H., Malhotra, A., and Tutundjian, S.: Assessing the impact of sand and dust storm on agriculture: Empirical evidence from Mongolia, PLoS. One., 18, e0269271, https://doi.org/10.1371/journal.pone.0269271, 2023.

Bueh, C., Zhuge, A., Xie, Z., Yong, M., and Purevjav, G.: The development of a powerful Mongolian cyclone on 14–15 March 2021: Eddy energy analysis, AOSL., 15, 100259, https://doi.org/10.1016/j.aosl.2022.100259, 2022.

C3S: Seasonal forecast subdaily data, available at: https://cds.climate.copernicus.eu/datasets/seasonal-original-single-levels?tab=download, last access: 21 October 2024.

Chen, S. Y., Zhao, D., Huang, J. P., He, J. Q., Chen, Y., Chen, J. Y., Bi, H. R., Lou, G. T., Du, S. K., Zhang, Y., and Yang, F.: Mongolia Contributed More than 42% of the Dust Concentrations in Northern China in March and April 2023, Adv. Atmos. Sci., 40, 1549–1557, https://doi.org/10.1007/s00376-023-3062-1, 2023a.

Chen, Y., Chen, S. Y., Zhou, J., Zhao, D., Bi, H. R., Zhang, Y., Alam, K., Yu, H. P., Yang, Y. X., and Chen, J. Y.: A super dust storm enhanced by radiative feedback, NPJ Clim. Atmos. Sci., 6, 90, https://doi.org/10.1038/s41612-023-00418-y, 2023b.

China National Environmental Monitoring Centre: Hourly PM_{10} concentration data, available at: https://quotsoft.net/air/, last access: 6 April 2024.

Copernicus Climate Change Service, Climate Data Store: Seasonal forecast subdaily data on pressure levels. Copernicus Climate Change Service (C3S) Climate Data Store (CDS) [data set], https://doi.org/10.24381/cds.50ed0a73, 2018.

Dulam, J., Shinoda, M., Kimura, R., Batbold, A., and Amarjargal, D.: Quantitative Analysis on Windblown Dust Concentrations of PM10 (PM2.5) during Dust Events in Mongolia, Aeolian Res., 14, 3–13, https://doi.org/10.1016/j.aeolia.2014.04.005, 2014.

ERA5: Reanalysis meteorological data, available at: https://cds.climate.copernicus.eu/datasets/reanalysis-era5-pressure-levels?tab=download, last access: 21 October 2024.

Gao, J., Ding, T., and Gao, H.: Dominant circulation pattern and moving path of the Mongolian Cyclone for the severe sand and dust storm in China, Atmos. Res., 301, 107272, https://doi.org/10.1016/j.atmosres.2024.107272, 2024.

Garratt J. R.: The Atmospheric Boundary Layer, Cambridge University Press, Cambridge, 1992.

Gui, K., Yao, W., Che, H., An, L., Zheng, Y., Li, L., Zhao, H., Zhang, L., Zhong, J., Wang, Y., and Zhang, X.: Record-breaking dust loading during two mega dust storm events over northern China in March 2021: aerosol optical and radiative properties and meteorological drivers, Atmos. Chem. Phys., 22, 7905–7932, https://doi.org/10.5194/acp-22-7905-2022, 2022.

Hersbach, H., Bell, B., Berrisford, P., Biavati, G., Horányi, A., Muñoz Sabater, J., Nicolas, J., Peubey, C., Radu, R., Rozum, I., Schepers, D., Simmons, A., Soci, C., Dee, D. and Thépaut, J-N: ERA5 hourly data on single levels from 1940 to present, Copernicus Climate Change Service (C3S) Climate Data Store (CDS) [data set], https://doi.org/10.24381/cds.adbb2d47, 2023.

Huang, J. P., Wang, T. H., Wang, W. C., Li, Z. Q., and Yan, H. R.: Climate effects of dust aerosols over East Asian arid and semiarid regions, J. Geophys. Res. Atmos., 119, 11398–11416, https://doi.org/10.1002/2014JD021796, 2014.

Krasnov, H., Katra, I., and Friger, M.: Increase in dust storm related PM10 concentrations: A time series analysis of 2001–2015, Environ. Pollut., 213, 36–42, https://doi.org/10.1016/j.envpol.2015.10.021, 2016.

Li, J. D., Hao, X., Liao, H., Yue, X., Li, H., Long, X., and Li, N: Predominant type of dust storms that influences air quality over northern China and future projections, Earth's Future, 10, e2022EF002649, https://doi.org/10.1029/2022EF002649, 2022.

Liu, J., Qian, Z., Jiang, X., and Zheng M.: A Study on Weather Types of Super Severe Dust Storms in North China, Plateau Meteor, 23, 540–547, 2004 (in Chinese).

Liu, S. K. and Liu, S. D.: Atmospheric dynamics, 2nd Edn., Peking University Press, Beijing, China, 143–147, 2011.

Lwin, K. S., Tobias, A., Chua, P. L., Yuan, L., Thawonmas, R., Ith, S., Htay, Z. W., Yu, L. S., Yamasaki, L., Roqué, M., Querol, X., Fussell, J. C., Nadeau, K. C., Stafoggia, M., Saliba, N. A., Sheng Ng, C. F., and Hashizume, M.: Effects of Desert Dust and Sandstorms on Human Health: A Scoping Review, GeoHealth, 7, e2022GH000728, https://doi.org/10.1029/2022GH000728, 2023.

Mu, F., Luiz, E. W., and Fiedler, S.: On the dynamics and air-quality impact of the exceptional East Asian dust outbreak in mid-March 2021, Atmos. Res., 292, 106846, https://doi.org/10.1016/j.atmosres.2023.106846, 2023.

NOAA: NDVI data, available at: https://www.ncei.noaa.gov/access/metadata/landing-page/bin/iso?id=gov.noaa.ncdc:C01558, last access: 20 May 2023.

Qian, W. H., Quan, L. S., and Shi, S. Y.: Variations of the Dust Storm in China and its Climatic Control, J. Clim., 15, 1216–1229, https://doi.org/10.1175/1520-0442(2002)015<1216:VOTDSI>2.0.CO;2, 2002.

Shao Y. P.: Physics and Modelling of Wind Erosion, 2nd Edn., Springer Dordrecht, 456 pp., https://doi.org/10.1007/978-1-4020-8895-7, 2008.

Shou S. W.: Synoptic Analysis, China Meteorological Press, Beijing, 361 pp., ISBN 9787502934576, 2006 (in Chinese).

Sugimoto, N., Shimizu, A., Matsui, I. and Nishikawa, M.: A method for estimating the fraction of mineral dust in particulate matter using $PM_{2.5}$-to-PM_{10} ratios, Particuology, 28, 114–120, https://doi.org/10.1016/j.partic.2015.09.005, 2016.

Takemi, T., and Seino, N.: Dust storms and cyclone tracks over the arid regions in east Asia in spring, J. Geophys. Res., 110, D18S11, https://doi.org/10.1029/2004JD004698, 2005.

Tian, Y., Pan, X. L., Jing, Y. J., Zhang, Y. T., Yao, W. J., Liu, H., Lei, S. D., and Wang, Z. F.: East Asia dust storms in spring 2021: Transport mechanisms and impacts on China, Atmos. Res., 290, 106773, https://doi.org/10.1016/j.atmosres.2023.106773, 2023.

Vermote, E.: NOAA Climate Data Record (CDR) of AVHRR Normalized Difference Vegetation Index (NDVI), Version 5, NOAA National Centers for Environmental Information [data set], https://doi.org/10.7289/V5ZG6QH9, 2019.

Wan, B., Kang, X., Zhang, J., Tong, Y., Tang, G., and Li, X.: Research on classification of dust and sand storm basic on particular concentration, Environ. Monit. China, 20, 8–11, https://doi.org/10.3969/j.issn.1002-6002.2004.03.003, 2004 (in Chinese).

Wang, S., Yu, Y., Zhang, X. X., Lu, H., Zhang, X. Y., and Xu., Z.: Weakened dust activity over China and Mongolia from 2001 to 2020 associated with climate change and land-use management, Environ. Res. Lett., 16, 124056, https://doi.org/10.1088/1748-9326/ac3b79, 2021.

Wang, Y. Q., Zhang, X. Y., Gong, S. L., Zhou, C. H., Hu, X. Q., Liu, H. L., Niu, T., and Yang, Y. Q.: Surface observation of sand and dust storm in East Asia and its application in CUACE/Dust, Atmos. Chem. Phys., 8, 545–553, https://doi.org/10.5194/acp-8-545-2008, 2008.

Wang, Y. Q., Zhang, X. Y., Sun, J. Y., Zhang, X. C., Che, H. Z., and Li, Y.: Spatial and temporal variations of the concentrations of PM_{10}, $PM_{2.5}$ and PM_1 in China, Atmos. Chem. Phys., 15, 13585–13598, https://doi.org/10.5194/acp-15-13585-2015, 2015.

Wiggs, G.F.S.: Sediment Mobilisation by the Wind, In Arid Zone Geomorphology: Process, Form and Change in Drylands, 3rd Edition, edited by: Thomas, D.S.G., Wiley, 455–486, https://doi.org/10.1002/9780470710777, 2011.

Wu, C. L., Lin, Z. H., He, J. X., Zhang, M. H., Liu, X. H., Zhang, R. J., and Brown, H.: A process-oriented evaluation of dust emission parameterizations in CESM: Simulation of a typical severe dust storm in East Asia, J. Adv. Model. Earth Syst., 8, 1432–1452, C10.1002/2016MS000723, 2016.

Wu, J., Li, C., Zhu, X. W., Qiu, Y. L., Tang, Y. X. and Ma, X. H.: Comparative analysis of meteorological factors and sand source conditions in sand and dust weather events in northern China during the spring of 2021 and 2022, Trans. Atmos. Sci., 46, 950–960, https://doi.org/10.13878/j.cnki.dqkxxb.20230313001, 2023 (in Chinese).

Yi, Z., Wang, Y., Chen, W., Guo, B., Zhang, B., Che, H., and Zhang, X.: Classification of the Circulation Patterns Related to Strong Dust Weather in China Using a Combination of the Lamb–Jenkinson and k-Means Clustering Methods, Atmosphere, 12, 1545, https://doi.org/10.3390/atmos12121545, 2021.

Yin, Z. C., Wan, Y., Zhang, Y. J., and Wang, H. J.: Why super sandstorm 2021 in North China?, Natl. Sci. Rev., 9, nwab165, https://doi.org/10.1093/nsr/nwab165, 2022.

Yin, Z. C., Huo, Q. Y., Ma, X. Q., Zhang, Y. J., Ma, X. H., and Wang., H. J.: Mechanisms of dust source accumulation and synoptic disturbance triggering the 2023 spring sandstorm in northern China, Trans. Atmos. Sci., 46, 321–331, https://doi.org/10.13878/j.cnki.dqkxxb.20230501007, 2023a (in Chinese).

Yin, Z. C., Zhou, B. T., Duan, M. K., Chen, H. S., and Wang, H. J.: Climate extremes become increasingly fierce in China, Innovation, 4, 100406, https://doi.org/10.1016/j.xinn.2023.100406, 2023b.

Yun, J., Jiang, X., Meng, X., Wu, X. and Ying, C.: Comparative Analyses on Some Statistic Characteristics between Cold Front and Mongolian Cyclone Duststorm Processes, Plateau Meteor, 32, 423–434, https://doi.org/10.7522/j.issn.1000-0534.2012.00041, 2013 (in Chinese).

Zhang, Lu., Fan, F., Wu, H., Zou, Y., Zhou, Z., Zhang, X. and Gao, S.: Diagnosis of sandstorm weather process and analysis of sand pollution transportation in northern China from 14th to 16th, March 2021, Acta Scientiae Circumstantiae, 42, 1–13, https://doi.org/10.13671/j.hjkxxb.2021.0452, 2022 (in Chinese).

Zhang, X. X., Lei, J. Q., Wu, S. X., Li, S. Y., Liu, L. Y., Wang, Z. F., Huang, S. Y., Guo, Y. H., Wang, Y. D., Tang, X., and Zhou, J.: Spatiotemporal evolution of aeolian dust in China: An insight into the synoptic records of 1984–2020 and nationwide practices to combat desertification, Land. Degrad. Dev., 34, 2005–2023, https://doi.org/10.1002/ldr.4585, 2023.

Zhang, Z. H. and Huisingh, D.: Combating desertification in China: Monitoring, control, management and revegetation, J. Clean. Prod., 182, 765–775, https://doi.org/10.1016/j.jclepro.2018.01.233, 2018.

Zhao, D., Chen, S. Y., and Chen, Y.: Comparative analysis of two typical dust storm processes over East Asia, J. Lanzhou Univ. Nat. Sci., 58, 313–322, https://doi.org/10.13885/j.issn.0455-2059.2022.03.005., 2022 (in Chinese).

Zhong, W. G., Yin, Z. C., and Wang, H. J.: The relationship between anticyclonic anomalies in northeastern Asia and severe haze in the Beijing–Tianjin–Hebei region, Atmos. Chem. Phys., 19, 5941–5957, https://doi.org/10.5194/acp-19-5941-2019, 2019.Ahmadzai, H., Malhotra, A., and Tutundjian, S.: Assessing the impact of sand and dust storm on agriculture: Empirical evidence from Mongolia, PLoS. One., 18, e0269271, https://doi.org/10.1371/journal.pone.0269271, 2023.

Bueh, C., Zhuge, A., Xie, Z., Yong, M., and Purevjav, G.: The development of a powerful Mongolian cyclone on 14–15 March 2021: Eddy energy analysis, AOSL., 15, 100259, https://doi.org/10.1016/j.aosl.2022.100259, 2022.

C3S: Seasonal forecast subdaily data, available at: https://cds.climate.copernicus.eu/cdsapp#!/dataset/10.24381/cds.50ed0a73?tab=overview, last access: 15 May 2024.

Chen, S. Y., Zhao, D., Huang, J. P., He, J. Q., Chen, Y., Chen, J. Y., Bi, H. R., Lou, G. T., Du, S. K., Zhang, Y., and Yang, F.: Mongolia Contributed More than 42% of the Dust Concentrations in Northern China in March and April 2023, Adv. Atmos. Sci., 40, 1549–1557, https://doi.org/10.1007/s00376-023-3062-1, 2023a.

Chen, Y., Chen, S. Y., Zhou, J., Zhao, D., Bi, H. R., Zhang, Y., Alam, K., Yu, H. P., Yang, Y. X., and Chen, J. Y.: A super dust storm enhanced by radiative feedback, NPJ Clim. Atmos. Sci., 6, 90, https://doi.org/10.1038/s41612-023-00418-y, 2023b.

China National Environmental Monitoring Centre: Hourly PM_{10} concentration data, available at: https://quotsoft.net/air/, last access: 6 April 2024.

Copernicus Climate Change Service, Climate Data Store: Seasonal forecast subdaily data on pressure levels. Copernicus Climate Change Service (C3S) Climate Data Store (CDS) [data set], https://doi.org/10.24381/cds.50ed0a73, 2018.

ERA5: Reanalysis meteorological data, available at: https://cds.climate.copernicus.eu/cdsapp#!/dataset/reanalysis-era5-pressure-levels?tab=overview, last access: 2 June 2023.

Filonchyk, M.: Characteristics of the severe March 2021 Gobi Desert dust storm and its impact on air pollution in China, Chemosphere, 287, 132219, https://doi.org/10.1016/j.chemosphere.2021.132219, 2022.

Gao, J., Ding, T., and Gao, H.: Dominant circulation pattern and moving path of the Mongolian Cyclone for the severe sand and dust storm in China, Atmos. Res., 301, 107272, https://doi.org/10.1016/j.atmosres.2024.107272, 2024.

Garratt J. R.: The Atmospheric Boundary Layer, Cambridge University Press, Cambridge, 1992.

Gui, K., Yao, W., Che, H., An, L., Zheng, Y., Li, L., Zhao, H., Zhang, L., Zhong, J., Wang, Y., and Zhang, X.: Record-breaking dust loading during two mega dust storm events over northern China in March 2021: aerosol optical and radiative properties and meteorological drivers, Atmos. Chem. Phys., 22, 7905–7932, https://doi.org/10.5194/acp-22-7905-2022, 2022.

Hersbach, H., Bell, B., Berrisford, P., Biavati, G., Horányi, A., Muñoz Sabater, J., Nicolas, J., Peubey, C., Radu, R., Rozum, I., Schepers, D., Simmons, A., Soci, C., Dee, D. and Thépaut, J-N: ERA5 hourly data on single levels from 1940 to present, Copernicus Climate Change Service (C3S) Climate Data Store (CDS) [data set], https://doi.org/10.24381/cds.adbb2d47, 2023.

Huang, J. P., Wang, T. H., Wang, W. C., Li, Z. Q., and Yan, H. R.: Climate effects of dust aerosols over East Asian arid and semiarid regions, J. Geophys. Res. Atmos., 119, 11398–11416, https://doi.org/10.1002/2014JD021796, 2014.

Krasnov, H., Katra, I., and Friger, M.: Increase in dust storm related PM10 concentrations: A time series analysis of 2001–2015, Environ. Pollut., 213, 36–42, https://doi.org/10.1016/j.envpol.2015.10.021, 2016.

Li, J. D., Hao, X., Liao, H., Yue, X., Li, H., Long, X., and Li, N: Predominant type of dust storms that influences air quality over northern China and future projections, Earth's Future, 10, e2022EF002649, https://doi.org/10.1029/2022EF002649, 2022.

Li, X., and Liu, X.: Relation of Spring Dust – Storm Activities in Northern China and Changes of Upper Westerlies, Plateau Meteor, 34, 1292–1300, https://doi.org/10.7522/j.issn.1000-0534.2014.00067, 2015 (in Chinese).

Liu, J., Qian, Z., Jiang, X., and Zheng M.: A Study on Weather Types of Super Severe Dust Storms in North China, Plateau Meteor, 23, 540–547, 2004 (in Chinese).

Liu, S. K. and Liu, S. D.: Atmospheric dynamics, 2nd Edn., Peking University Press, Beijing, China, 143–147, 2011.

Lwin, K. S., Tobias, A., Chua, P. L., Yuan, L., Thawonmas, R., Ith, S., Htay, Z. W., Yu, L. S., Yamasaki, L., Roqué, M., Querol, X., Fussell, J. C., Nadeau, K. C., Stafoggia, M., Saliba, N. A., Sheng Ng, C. F., and Hashizume, M.: Effects of Desert Dust and Sandstorms on Human Health: A Scoping Review, GeoHealth, 7, e2022GH000728, https://doi.org/10.1029/2022GH000728, 2023.

Mu, F., Luiz, E. W., and Fiedler, S.: On the dynamics and air-quality impact of the exceptional East Asian dust outbreak in mid-March 2021, Atmos. Res., 292, 106846, https://doi.org/10.1016/j.atmosres.2023.106846, 2023.

NOAA: NDVI data, available at: https://www.ncei.noaa.gov/access/metadata/landing-page/bin/iso?id=gov.noaa.ncdc:C01558, last access: 20 May 2023.

Qian, W. H., Quan, L. S., and Shi, S. Y.: Variations of the Dust Storm in China and its Climatic Control, J. Clim., 15, 1216–1229, https://doi.org/10.1175/1520-0442(2002)015<1216:VOTDSI>2.0.CO;2, 2002.

Shao Y. P.: Physics and Modelling of Wind Erosion, 2nd Edn., Springer Dordrecht, 456 pp., https://doi.org/10.1007/978-1-4020-8895-7, 2008.

Shou S. W.: Synoptic Analysis, China Meteorological Press, Beijing, 361 pp., ISBN 9787502934576, 2006 (in Chinese).

Takemi, T., and Seino, N.: Dust storms and cyclone tracks over the arid regions in east Asia in spring, J. Geophys. Res., 110, D18S11, https://doi.org/10.1029/2004JD004698, 2005.

Tian, Y., Pan, X. L., Jing, Y. J., Zhang, Y. T., Yao, W. J., Liu, H., Lei, S. D., and Wang, Z. F.: East Asia dust storms in spring 2021: Transport mechanisms and impacts on China, Atmos. Res., 290, 106773, https://doi.org/10.1016/j.atmosres.2023.106773, 2023.

Vermote, E.: NOAA Climate Data Record (CDR) of AVHRR Normalized Difference Vegetation Index (NDVI), Version 5, NOAA National Centers for Environmental Information [data set], https://doi.org/10.7289/V5ZG6QH9, 2019.

Wang, S., Yu, Y., Zhang, X. X., Lu, H., Zhang, X. Y., and Xu., Z.: Weakened dust activity over China and Mongolia from 2001 to 2020 associated with climate change and land use management, Environ. Res. Lett., 16, 124056, https://doi.org/10.1088/1748-9326/ac3b79, 2021.

Wiggs, G.F.S.: Sediment Mobilisation by the Wind, In Arid Zone Geomorphology: Process, Form and Change in Drylands, 3rd Edition, edited by: Thomas, D.S.G., Wiley, 455–486, https://doi.org/10.1002/9780470710777, 2011.

Wu, C. L., Lin, Z. H., He, J. X., Zhang, M. H., Liu, X. H., Zhang, R. J., and Brown, H.: A process-oriented evaluation of dust emission parameterizations in CESM: Simulation of a typical severe dust storm in East Asia, J. Adv. Model. Earth Syst., 8, 1432–1452, C10.1002/2016MS000723, 2016.

Wu, J., Li, C., Zhu, X. W., Qiu, Y. L., Tang, Y. X. and Ma, X. H.: Comparative analysis of meteorological factors and sand source conditions in sand and dust weather events in northern China during the spring of 2021 and 2022, Trans. Atmos. Sci., 46, 950–960, https://doi.org/10.13878/j.cnki.dqkxxb.20230313001, 2023 (in Chinese).

Yi, Z., Wang, Y., Chen, W., Guo, B., Zhang, B., Che, H., and Zhang, X.: Classification of the Circulation Patterns Related to Strong Dust Weather in China Using a Combination of the Lamb–Jenkinson and k-Means Clustering Methods, Atmosphere, 12, 1545, https://doi.org/10.3390/atmos12121545, 2021.

Yin, Z. C., Wan, Y., Zhang, Y. J., and Wang, H. J.: Why super sandstorm 2021 in North China?, Natl. Sci. Rev., 9, nwab165, https://doi.org/10.1093/nsr/nwab165, 2022.

Yin, Z. C., Huo, Q. Y., Ma, X. Q., Zhang, Y. J., Ma, X. H., and Wang., H. J.: Mechanisms of dust source accumulation and synoptic disturbance triggering the 2023 spring sandstorm in northern China, Trans. Atmos. Sci., 46, 321–331, https://doi.org/10.13878/j.cnki.dqkxxb.20230501007, 2023a (in Chinese).

Yin, Z. C., Zhou, B. T., Duan, M. K., Chen, H. S., and Wang, H. J.: Climate extremes become increasingly fierce in China, Innovation, 4, 100406, https://doi.org/10.1016/j.xinn.2023.100406, 2023b.

Yun, J., Jiang, X., Meng, X., Wu, X. and Ying, C.: Comparative Analyses on Some Statistic Characteristics between Cold Front and Mongolian Cyclone Duststorm Processes, Plateau Meteor, 32, 423–434, https://doi.org/10.7522/j.issn.1000-0534.2012.00041, 2013 (in Chinese).

Zhang, Lu., Fan, F., Wu, H., Zou, Y., Zhou, Z., Zhang, X. and Gao, S.: Diagnosis of sandstorm weather process and analysis of sand pollution transportation in northern China from 14th to 16th, March 2021, Acta Scientiae Circumstantiae, 42, 1–13, https://doi.org/10.13671/j.hjkxxb.2021.0452, 2022 (in Chinese).

Zhang, X. X., Lei, J. Q., Wu, S. X., Li, S. Y., Liu, L. Y., Wang, Z. F., Huang, S. Y., Guo, Y. H., Wang, Y. D., Tang, X., and Zhou, J.: Spatiotemporal evolution of aeolian dust in China: An insight into the synoptic records of 1984–2020 and nationwide practices to combat desertification, Land. Degrad. Dev., 34, 2005–2023, https://doi.org/10.1002/ldr.4585, 2023.

Zhang, Y., Yin, Z., Wang, H., and He, S.: 2020/21 record-breaking cold waves in east of China enhanced by the 'Warm Arctic-Cold Siberia' pattern, Environ. Res. Lett., 16, 094040, https://doi.org/10.1088/1748-9326/ac1f46, 2021.

Zhang, Z. H. and Huisingh, D.: Combating desertification in China: Monitoring, control, management and revegetation, J. Clean. Prod., 182, 765–775, https://doi.org/10.1016/j.jclepro.2018.01.233, 2018.

Zhao, D., Chen, S. Y., and Chen, Y.: Comparative analysis of two typical dust storm processes over East Asia, J. Lanzhou Univ. Nat. Sci., 58, 313–322, https://doi.org/10.13885/j.issn.0455-2059.2022.03.005., 2022 (in Chinese).

Zhong, W. G., Yin, Z. C., and Wang, H. J.: The relationship between anticyclonic anomalies in northeastern Asia and severe haze in the Beijing–Tianjin–Hebei region, Atmos. Chem. Phys., 19, 5941–5957, https://doi.org/10.5194/acp-19-5941-2019, 2019.

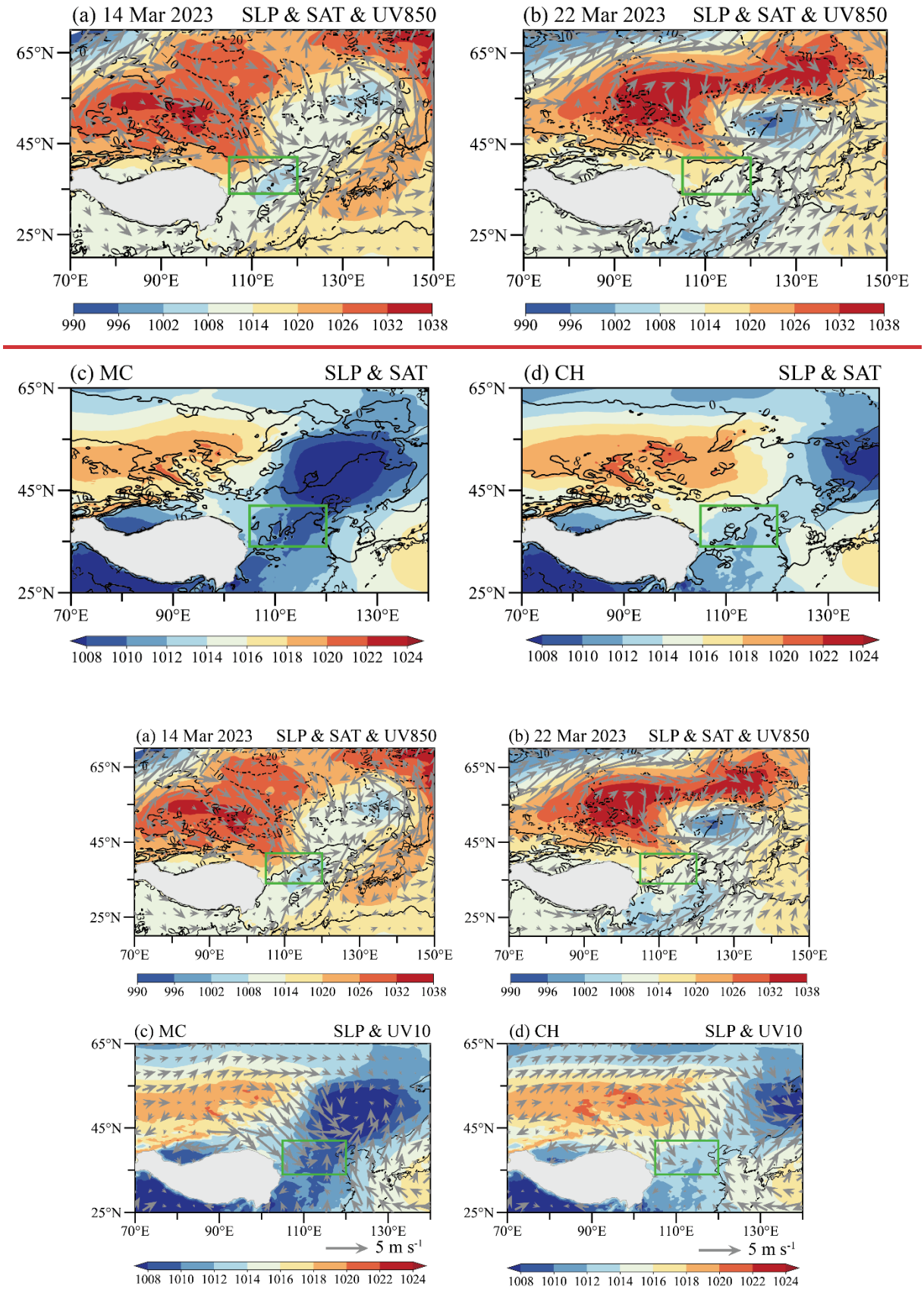

Figure S1. (a) SLP (shading, units: hPa), SAT (contour, units: ℃) and UV850 (vectors, units: m s^{-1}) on 14 March 2023. Panel (b) is the same as (a) but for 22 March 2023. ~~(c) Composite~~

~~SLP (shading, units: hPa) and SAT (contour, units: °C) during MC days. Panel (d) is the same as (c) but for CH days.~~ (c) Composites of original SLP (shading, units: hPa) and UV10 (vectors, units: m s^{-1}) during MC days. Panel (d) is the same as panel (c) but for CH days. The green boxes in panel (a)–(~~d~~d) represent NC.

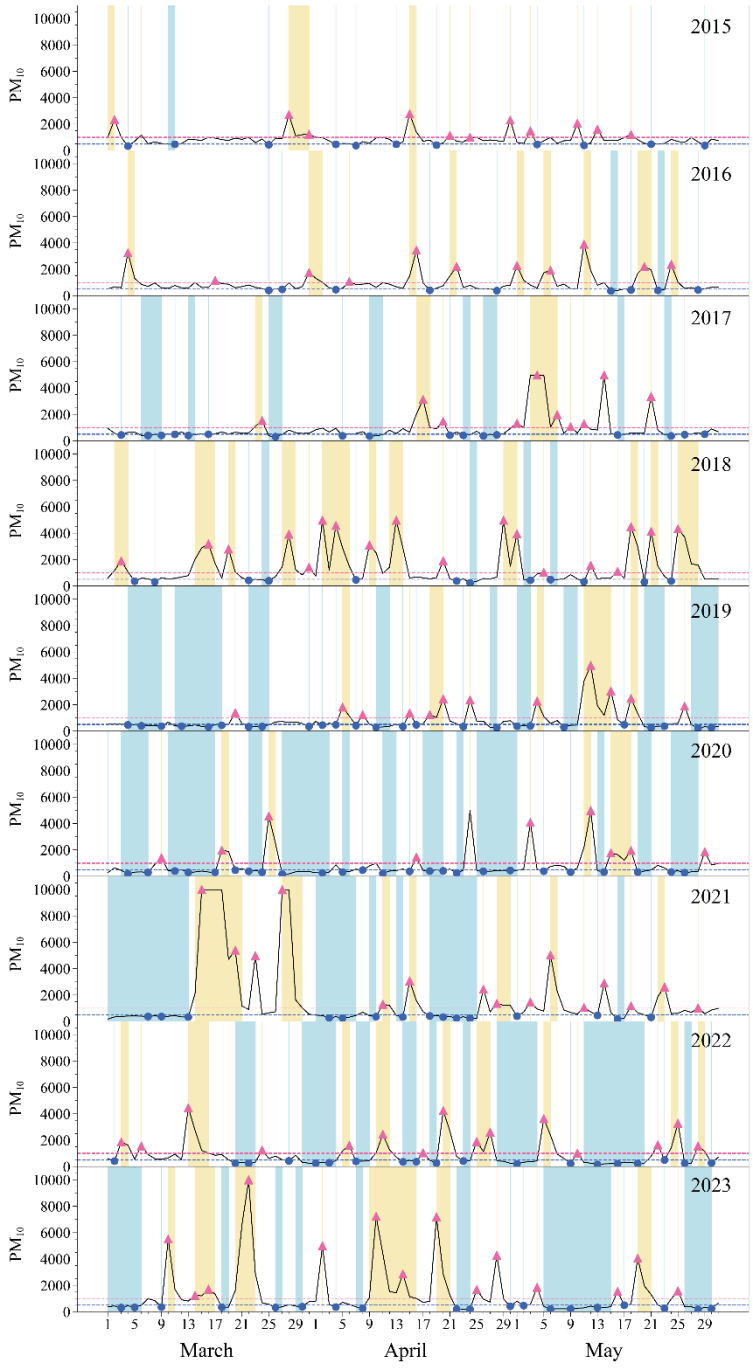

Figure S2. Variations of observed daily maximum PM_{10} concentrations (black lines, unit: μg m^{-3}). The yellow shadings represent periods of PM_{10} concentrations exceeding 1000 μg m^{-3}, while the blue shadings represent periods with PM_{10} concentrations below 500 μg m^{-3}. The pink triangles represent the selected Dust days, while the blue dots represent the selected Non-

Dust days. Dashed lines (blue and pink) depict threshold values for PM_{10} concentration at 500 and 1000 μg m^{-3} respectively.

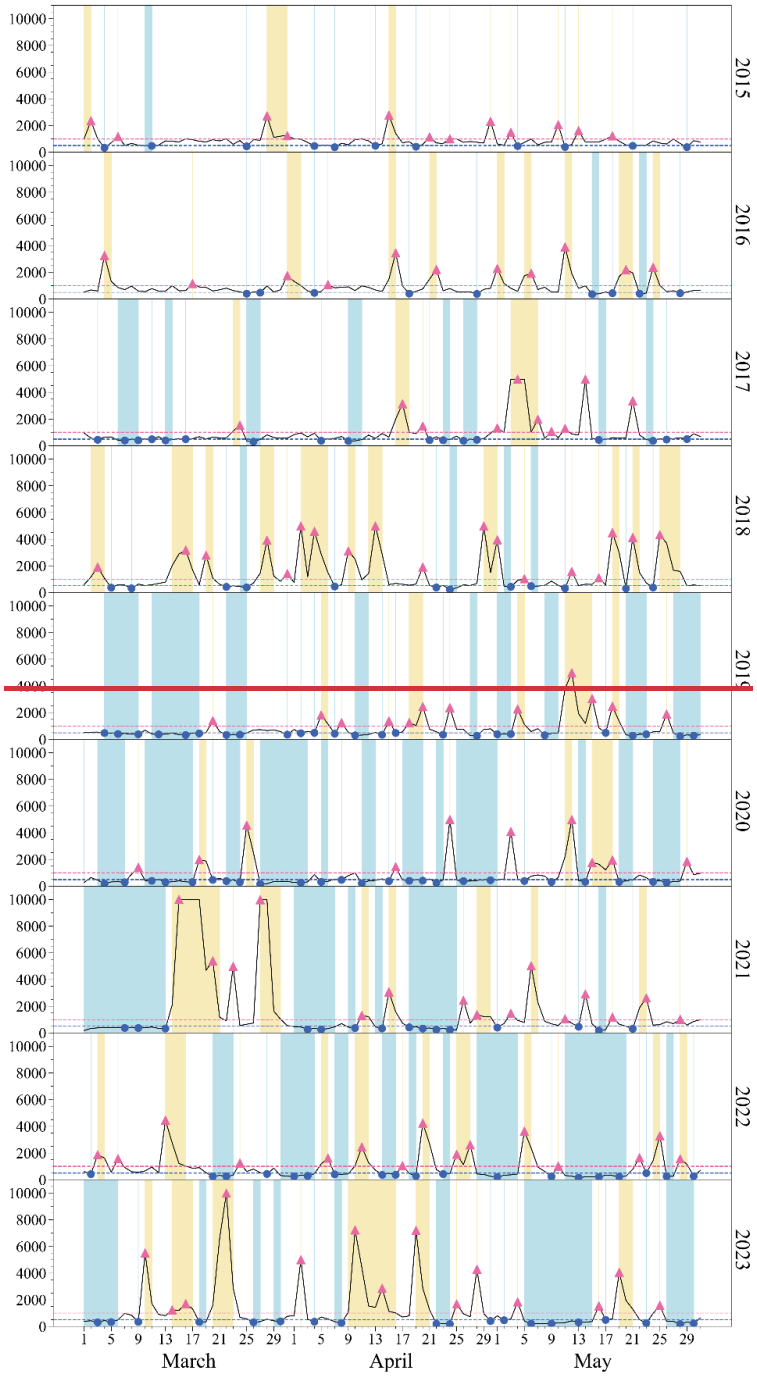

Figure S2. Variations of observed daily maximum PM_{10} concentrations (black lines, unit: μg m^{-3}) over NC in spring from 2015 to 2023. The yellow shadings represent periods of PM_{10} concentrations exceeding 1000 μg m^{-3}, while the blue shadings represent periods with PM_{10} concentrations below 500 μg m^{-3}. The pink triangles represent the maximum PM_{10} concentrations exceeding 1000 μg m^{-3}, while the blue dots represent the minimum PM_{10} concentrations below 500 μg m^{-3}. Dashed lines (blue and pink) depict threshold values for PM_{10} concentration at 500 and 1000 μg m^{-3} respectively.

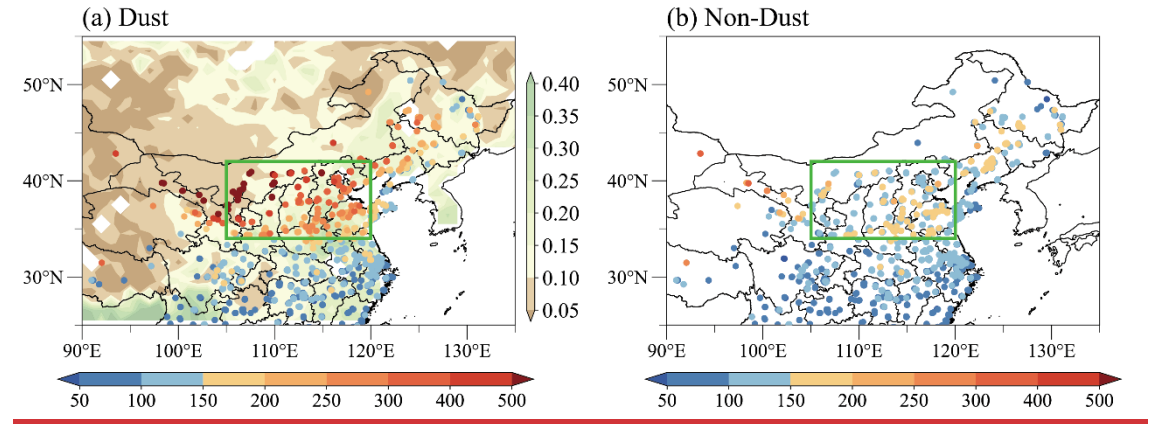

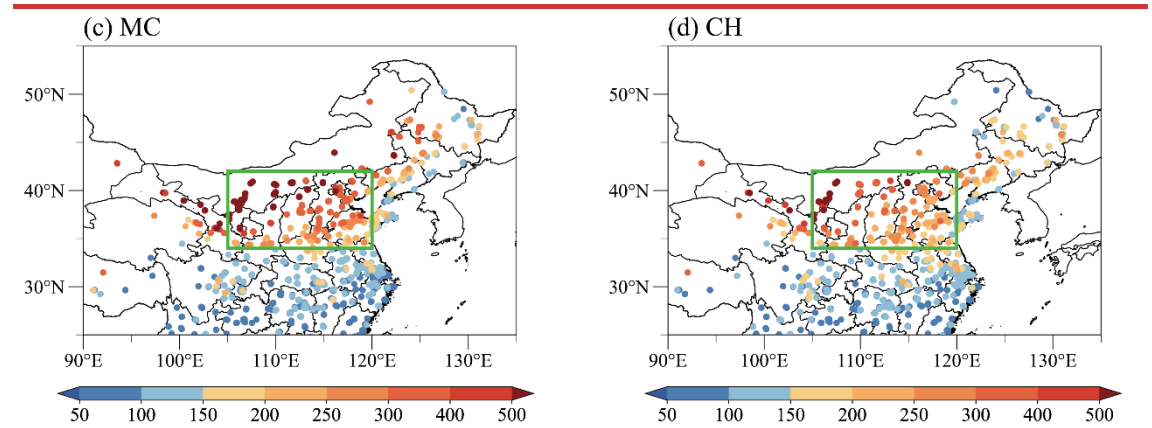

26

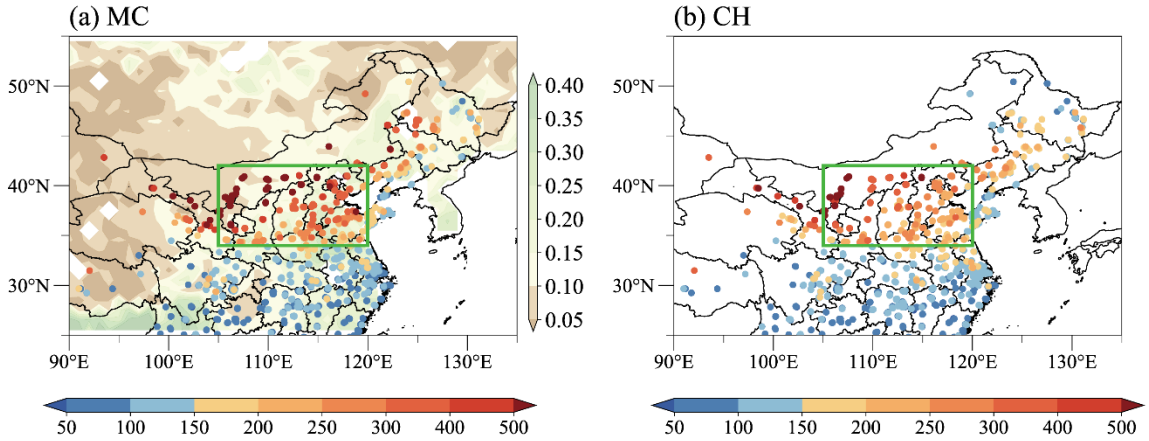

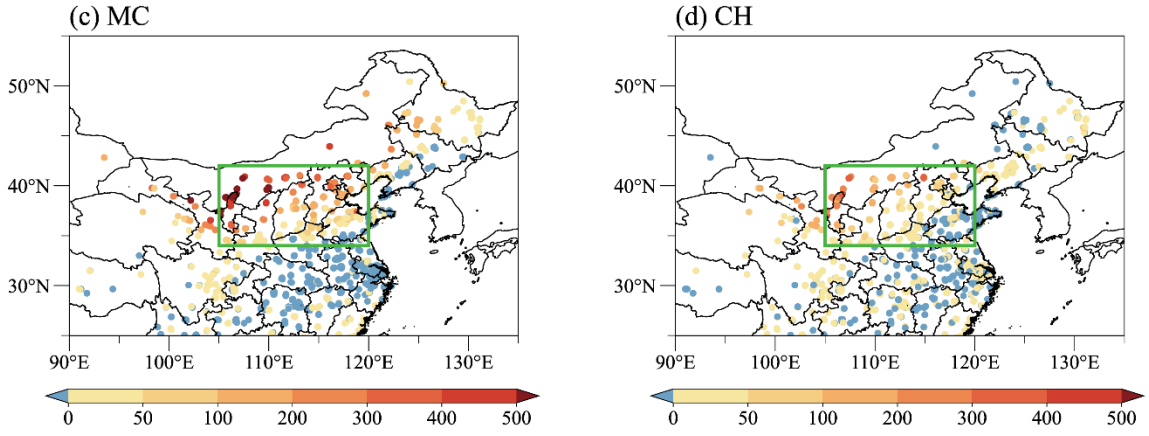

27

28 **Figure ~~S3~~S3.** (a) Composite distribution of observed daily maximum PM_{10} concentrations

(scatter, unit: μg m^{-3}) during MC days. Panel (b) is the same as (a) but for CH days. The shading in panel (a) indicates NDVI in March 2023. (c) Composite distribution of observed daily maximum PM_{10} concentrations anomalies (scatter, unit: μg m^{-3}) during MC days. Panel (d) is the same as (a) but for CH days. The green boxes in panel (a)–(d) represent NC.

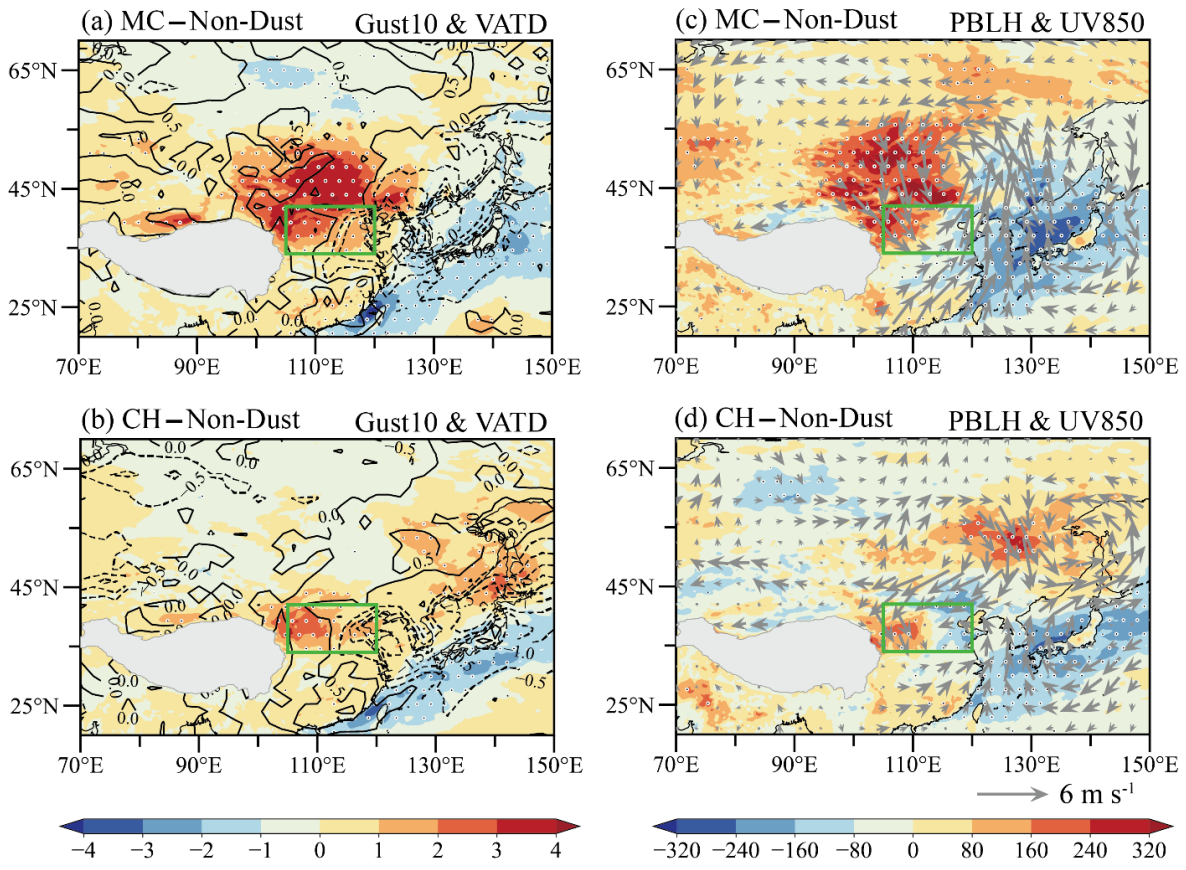

Figure S4. (a) Composite differences of Gust10 (shading, units: m s^{-1}) and VATD (contour, units: K) during MC days relative to Non-Dust days. White dots indicate that the differences of Gust10 exceed the 95% confidence level. Panel (b) is the same as panel (a) but for CH days. (c) Composite differences of PBLH (shading, units: m) during MC days relative to Non-Dust days and composite anomalies of UV850 (vectors, units: m s^{-1}). White dots indicate that the differences of PBLH exceed the 95% confidence level. Panel (d) is the same as panel (c) but for CH days. The green boxes in panel (a)–(d) represent NC.

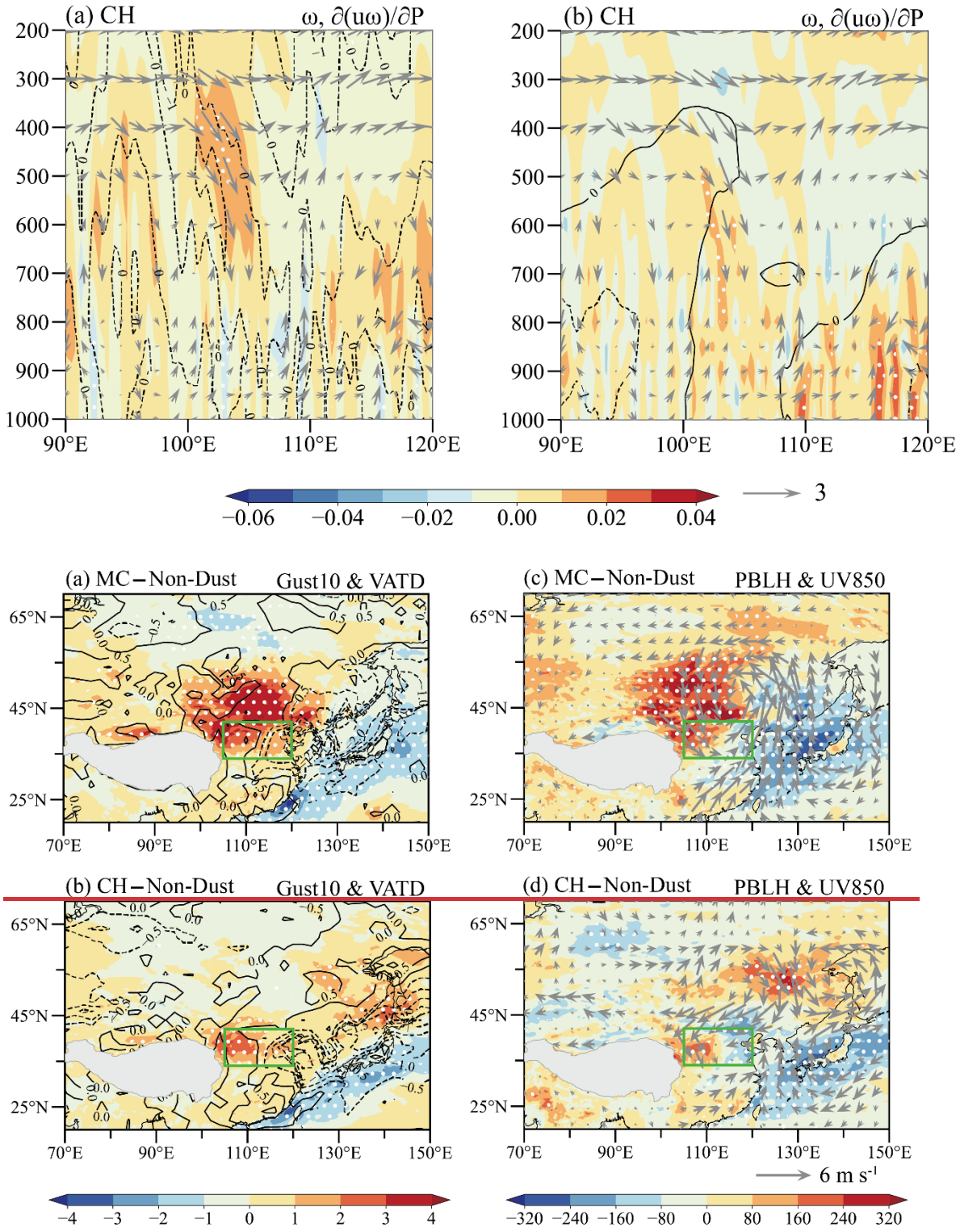

~~Figure S4.~~ ~~(a) Composite differences of Gust10 (shading, units: m s^{-1}) and VATD (contour, units: K) during MC days relative to Non-Dust days. White dots indicate that the differences of Gust10 exceed the 95% confidence level. Panel (b) is the same as panel (a) but for CH days. (c) Composite differences of PBLH (shading, units: m) during MC days relative to Non-Dust days and composite anomalies of UV850 (vectors, units: m s^{-1}). White dots indicate that the differences of PBLH exceed the 95% confidence level. Panel (d) is the same as panel (c) but~~

~~for CH days. The green boxes in panel (a)–(d) represent NC.~~

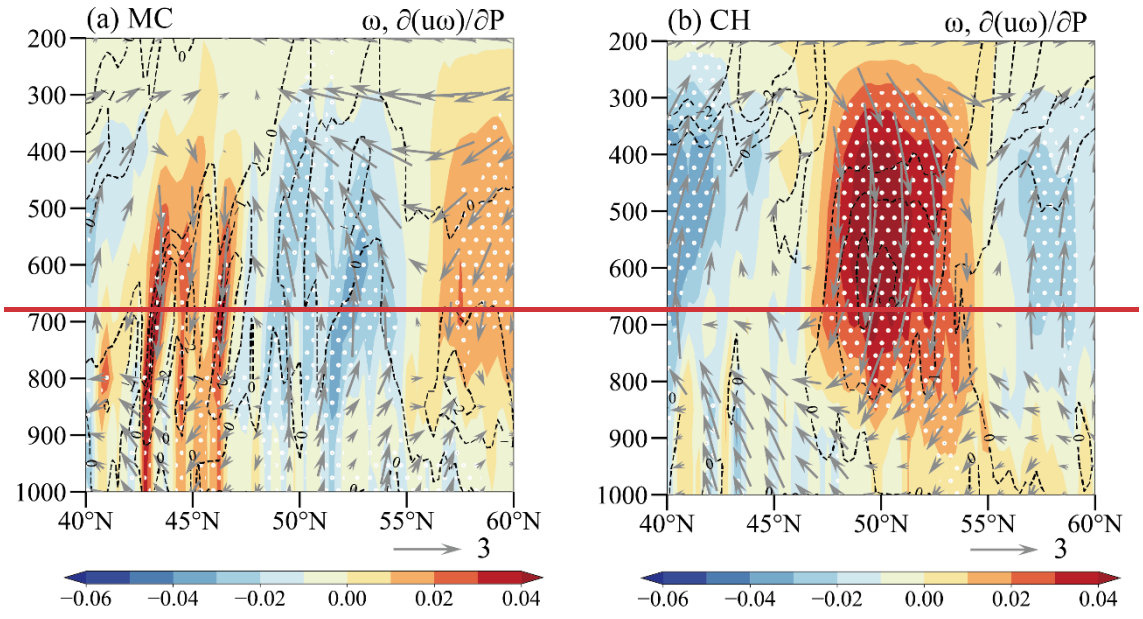

Figure S5. Composite anomalies of zonal component of the vertical circulation average over 40–60°N, 90–120°E during CH days: (a) The variables include ω (shading, units: Pa s^{-1}) and downward transport of westerly momentum (<0, dashed contour, units: 10^{-3} m s^{-2}). White dots indicate that ω anomalies exceed the 95% confidence level. The vectors represent ω (magnified 100 times) and zonal wind. (b) The variables include divergence (shading, units: 10^{-5} s^{-1}) and q (contour, units: 10^{-4} kg kg^{-1}). White dots indicate that divergence anomalies exceed the 95% confidence level. The vectors represent ω (magnified 100 times) and zonal wind.

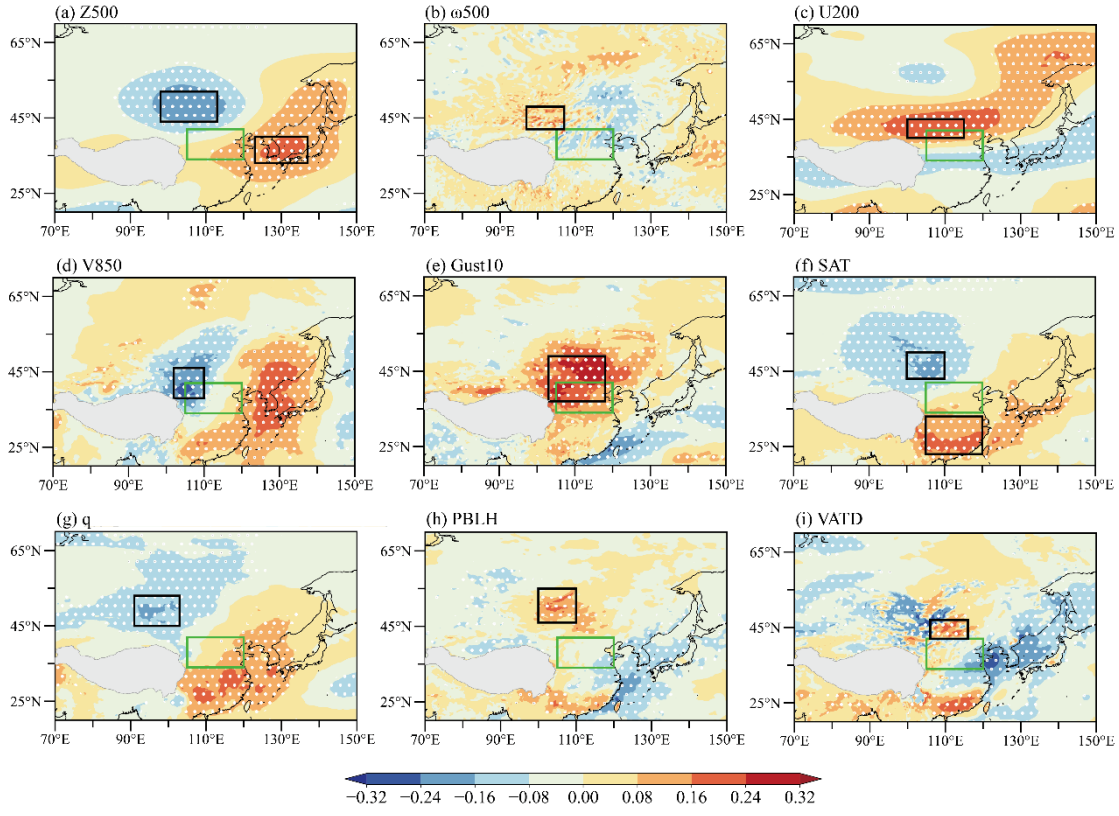

Figure ~~S6~~S6. Correlation coefficients of observed daily maximum PM_{10} concentrations over NC with daily ~~mean~~ (a) Z500, (b) ω500, (c) U200, (d) V850, (e) Gust10, (f) SAT, (g) q, (h) PBLH, and (i) VATD in spring from 2015 to 2023. White dots indicate that correlation coefficients exceed the 95% confidence level. The green boxes in panel (a)–(i) represent NC. The black boxes in panel (a)–(i) represent the regions for calculating the indices in Table 1 respectively ~~(Table 1)~~.

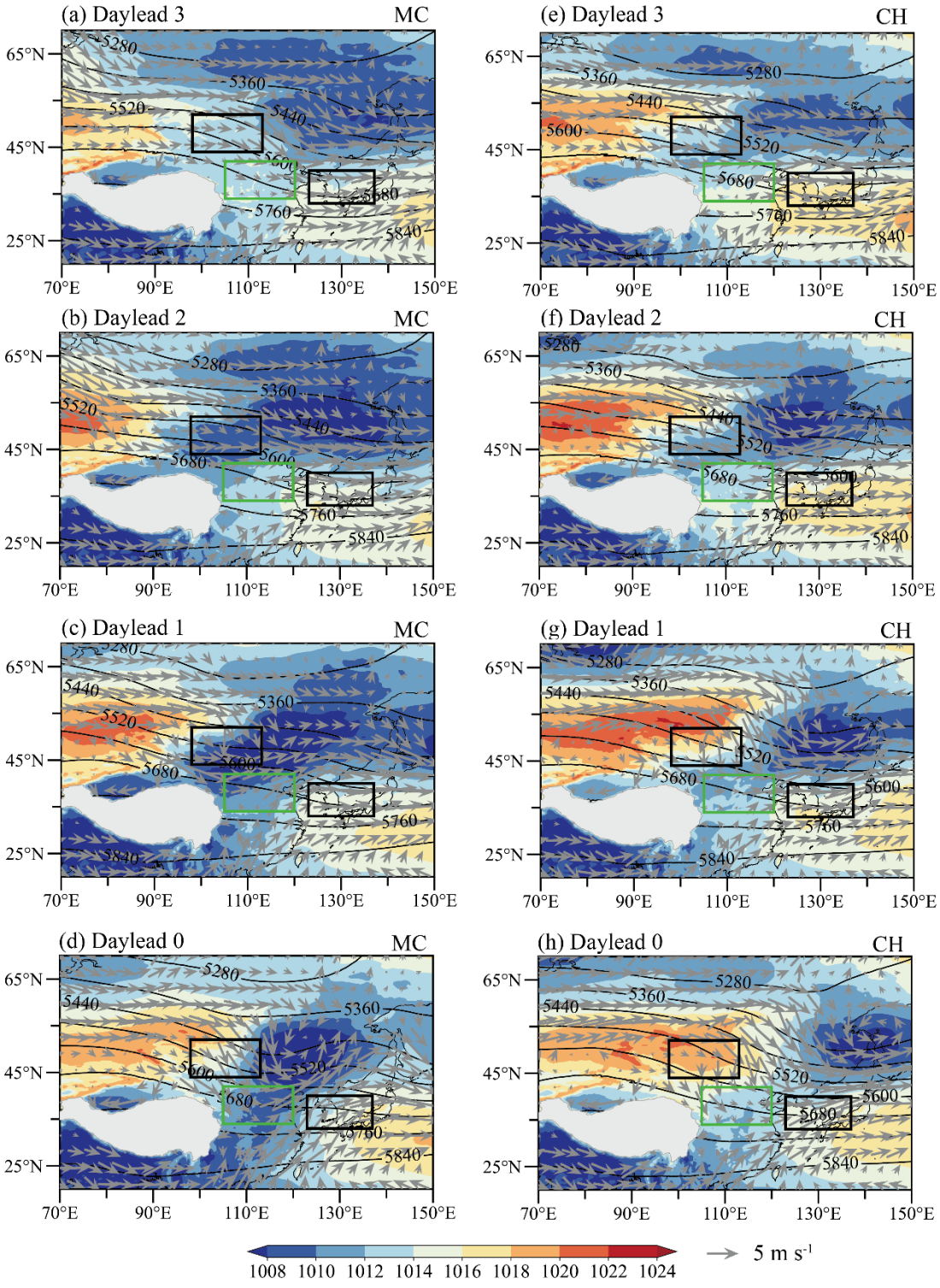

Figure S7. (a)–(d) Lead composite evolution of original Z500 (contour, unit: gpm), SLP (shading, unit: hPa), and UV850 (vectors, units: m s^{-1}) during MC days. Panel (e)–(h) are the same as panel (a)−(d) but for CH days. The green boxes in panel (a)–(h) represent NC, while the black boxes represent the region for calculating I_ACA-CA.

~~**Figure S5.** (a) Composite anomalies of meridional component of the vertical circulation average over 40–60° N, 90–120° E during MC days. The variables include ω (shading, units: Pa s^{-1}) and downward transport of westerly momentum (<0, dashed contour, units: 10^{-3} m s^{-2}). White dots indicate that ω anomalies exceed the 95% confidence level. The vectors represent ω (magnified 100 times) and zonal wind. Panel (b) is the same as (a) but for CH days.~~